This Accepted Manuscript has not been copyedited and formatted. The final version may differ from this version.

JNeurosci
THE JOURNAL OF NEUROSCIENCE

Research Articles: Neurobiology of Disease

Maternal and Early Postnatal Immune Activation Produce Dissociable Effects on Neurotransmission in mPFC-Amygdala Circuits

Yan Li[1], Galen Missig[1], Beate C. Finger[1], Samantha M. Landino[1], Abigail J. Alexander[1], Emery Mokler[1], James Robbins[1], Yunona Manasian[1], Woori Kim[1], Kwang-Soo Kim[1], Christopher J. McDougle[2], William A. Carlezon[1] and Vadim Y. Bolshakov[1]

[1]*Department of Psychiatry, McLean Hospital, Harvard Medical School, Belmont, MA 02478, USA*
[2]*Lurie Center for Autism, Massachusetts General Hospital, Harvard Medical School, Lexington, MA 02421, USA*

DOI: 10.1523/JNEUROSCI.3642-17.2018

Received: 27 December 2017

Revised: 13 February 2018

Accepted: 21 February 2018

Published: 28 February 2018

Author contributions: K.-S.K., C.J.M., W.A.C.J., and V.B. designed research; Y.L., G.M., B.C.F., S.M.L., A.J.A., E.M., J.R., Y.M., and W.K. performed research; Y.L., G.M., B.C.F., S.M.L., A.J.A., E.M., J.R., Y.M., and W.K. analyzed data; K.-S.K., C.J.M., W.A.C.J., and V.B. wrote the paper.

Conflict of Interest: The authors declare no competing financial interests.

We thank the Robert and Donna Landreth Family Foundation and the Nancy Lurie Marks Family Foundation for their generous support of this project.

Correspondence should be addressed to: Vadim Y. Bolshakov, , McLean Hospital, Harvard Medical School, Belmont, MA 02478, Tel: 617-855-3171, Email: vadimb@mclean.harvard.edu, or to: William A. Carlezon, Jr., McLean Hospital, Harvard Medical School, Belmont, MA 02478, Tel: 617-855-2021, Email: bcarlezon@mclean.harvard.edu

Cite as: J. Neurosci ; 10.1523/JNEUROSCI.3642-17.2018

Alerts: Sign up at www.jneurosci.org/cgi/alerts to receive customized email alerts when the fully formatted version of this article is published.

Accepted manuscripts are peer-reviewed but have not been through the copyediting, formatting, or proofreading process.

Copyright © 2018 the authors

JNeurosci Accepted Manuscript

JNeurosci Accepted Manuscript

Maternal and Early Postnatal Immune Activation Produce Dissociable Effects on Neurotransmission in mPFC-Amygdala Circuits

Yan Li[1], Galen Missig[1], Beate C. Finger[1], Samantha M. Landino[1], Abigail J. Alexander[1], Emery Mokler[1], James Robbins[1], Yunona Manasian[1], Woori Kim[1], Kwang-Soo Kim[1], Christopher J. McDougle[2], William A. Carlezon, Jr[1*], and Vadim Y. Bolshakov[1*]

[1]Department of Psychiatry, McLean Hospital
Harvard Medical School
Belmont, MA 02478, USA

[2]Lurie Center for Autism, Massachusetts General Hospital
Harvard Medical School
Lexington, MA 02421, USA

Correspondence should be addressed to:
Vadim Y. Bolshakov
McLean Hospital
Harvard Medical School
Belmont, MA 02478
Tel: 617-855-3171
Email: vadimb@mclean.harvard.edu

or to:

William A. Carlezon, Jr.
McLean Hospital
Harvard Medical School
Belmont, MA 02478
Tel: 617-855-2021
Email: bcarlezon@mclean.harvard.edu

[*]Equivalent senior authorship roles

Text pages – 42 pages
Figures – 8 figures
Abstract – 250 words
Introduction – 649 words
Discussion – 964 words

Abbreviated Title: Role of Immune Activation in Autism

Acknowledgements: We thank the Robert and Donna Landreth Family Foundation and the Nancy Lurie Marks Family Foundation for their generous support of this project.

The authors declare no competing financial interests.

JNeurosci Accepted Manuscript

Abstract

Inflammatory processes may be involved in the pathophysiology of neuropsychiatric illnesses including Autism Spectrum Disorder (ASD). Evidence from studies in rodents indicates that immune activation during early development can produce core features of ASD (social interaction deficits, dysregulation of communication, increases in stereotyped behaviors and anxiety), although the neural mechanisms of these effects are not thoroughly understood. We treated timed-pregnant mice with polyinosinic:polycytidylic acid (Poly I:C), which simulates a viral infection, or vehicle on gestational day 12.5 to produce maternal immune activation (MIA). Male offspring received either vehicle or lipopolysaccharide (LPS), which simulates a bacterial infection, on postnatal day 9 to produce postnatal immune activation (PIA). We then used optogenetics to address the possibility that early developmental immune activation causes persistent alterations in the flow of signals within the medial prefrontal cortex (mPFC) to basolateral amygdala (BLA) pathway, a circuit implicated in ASD. We found that our MIA regimen produced increases in synaptic strength in glutamatergic projections from the mPFC to the BLA. In contrast, our PIA regimen produced decreases in feed-forward GABAergic inhibitory postsynaptic responses resulting from activation of local circuit interneurons in the BLA by mPFC-originating fibers. Both effects were seen together when the regimens were combined. Changes in the balance between excitation and inhibition were differentially translated into the modified spike output of BLA neurons. Our findings raise the possibility that prenatal and postnatal immune activation may affect different cellular targets within brain circuits that regulate some of the core behavioral signs of conditions such as ASD.

JNeurosci Accepted Manuscript

Significance Statement

Immune system activation during prenatal and early postnatal development may contribute to the development of Autism Spectrum Disorder (ASD). Combining optogenetic approaches and behavioral assays that reflect core features of ASD (anxiety, decreased social interactions), we uncovered mechanisms by which the ASD-associated behavioral impairments induced by immune activation could be mediated at the level of interactions within brain circuits implicated in control of emotion and motivation (mPFC and BLA, specifically). In this article, we present evidence that prenatal and postnatal immune activation can have different cellular targets in the brain, providing support to the notion that the etiology of ASD may be linked to the excitation/inhibition imbalance in the brain affecting the signal flow within relevant behavior-driving neural microcircuits.

JNeurosci Accepted Manuscript

Accumulating evidence suggests that the immune system is involved in neuropsychiatric conditions including autism spectrum disorder (ASD) (Miller et al., 2017). ASD comprises a group of neurodevelopmental disorders with distinctive behavioral manifestations and complex underlying mechanisms (Markram and Markram, 2010). The contribution of genetic factors to some forms of ASD is well established (Abrahams and Geschwind, 2008; Betancur, 2011; O'Roak et al., 2012; Talkowski et al., 2014). However, environmental factors, including those that trigger immune responses, may also play a role in the etiology of ASD (Onore et al., 2012; McDougle et al., 2015; Lombardo et al., 2017; Meltzer and Van de Water, 2017). Several studies have shown that viral infection during the second-trimester of pregnancy is associated with an increased risk of ASD (Patterson, 2009; Atladótir et al., 2010; Zerbo et al., 2011; Knuesel et al., 2014; Patel et al., 2017). Consistent with the results of studies in humans, immune system activation in laboratory animals can recapitulate key aspects of ASD, supporting the notion that immunoactivation in the brain could lead to the development of functional abnormalities characteristic of ASD (Smith et al., 2007; Sangha et al., 2014; Canetta et al., 2016; Choi et al., 2016).

It is becoming increasingly clear that ASD is a neural network phenomenon that may reflect dysregulation of functional interactions between brain regions, controlling specific behavioral domains. Typically, aberrant social interactions, communication deficits, and increases in stereotyped behaviors are considered to be the primary diagnostic features of ASD, but these signs are frequently co-morbid with other features including enhanced anxiety. The neurocircuits underlying social interaction and anxiety-related behaviors

JNeurosci Accepted Manuscript

110 are well defined and include the medial prefrontal cortex (mPFC) and the amygdala
111 (AMG) (Baron-Cohen et al., 1999; Markram and Markram, 2010). Accordingly, there is
112 increasing interest in the possibility that ASD-associated behavioral impairments may
113 be linked to dysfunction within these neural circuits. It has been demonstrated in
114 genetic and valproic acid exposure models that the development of ASD-like behavioral
115 signs is associated with hyperconnectivity within the mPFC (Rinaldi et al., 2008; Sui and
116 Chen, 2012; Testa-Silva et al., 2012). This could increase activation of target areas
117 receiving projections from the mPFC, including the AMG. Because the AMG is a key
118 component of the brain circuits underlying anxiety-related behaviors (LeDoux, 2000),
119 increased mPFC-AMG functional connectivity might contribute to features of anxiety
120 and social avoidance seen in ASD.
121
122 Previous studies have implicated the activity of projections from the mPFC to the AMG
123 in control of anxiety and fear (Maren and Quirk, 2004; Pape and Pare, 2010). It remains
124 unknown, however, whether the development of ASD features is associated with altered
125 neurotransmission in the mPFC-BLA pathway. Using optogenetic techniques (Boyden
126 et al., 2005), we addressed this question in a “two hit” mouse model (Harvey and Boksa,
127 2012; Giovanoli et al., 2013), exploring the possibility that early developmental immune
128 activation can increase the prevalence of ASD-associated dysfunctions (Mrozek-Budzyn
129 et al., 2013; Hadjkacem et al., 2016). In this model, mice received a maternal immune
130 activation (MIA) challenge on embryonic day 12.5 (E12.5) with polyinosinic:polycytidylic
131 acid (Poly I:C)—a toll-like receptor 3 [TLR3] agonist simulating an innate immune
132 response to a virus—with or without a subsequent postnatal immune activation (PIA)

JNeurosci Accepted Manuscript

challenge with lipopolysaccharide (LPS)—a TLR4 agonist simulating an innate immune response to bacteria—on postnatal day 9 (PND9) (Smith et al., 2007; Kawai and Akira, 2008; Reisinger et al., 2015; Canetta et al., 2016; Choi et al., 2016; Custódio et al., 2017; Patel et al., 2017). This approach aligns with TLR expression patterns (Barak et al., 2014) and infection risk factors seen in humans (Bilbo et al., 2009). We then examined neurotransmission in mPFC-BLA projections in the treatment groups. We found that our MIA regimen significantly enhanced glutamatergic synaptic transmission in mPFC-BLA projections, whereas our PIA regimen significantly diminished feed-forward inhibition in the same pathway, suggesting that these immune challenges act upon different cellular targets in the brain.

Materials and Methods

Animal model of maternal and postnatal immunoactivation. The McLean Hospital Institutional Animal Care and Use Committee approved all animal procedures in this study. Timed pregnant Jackson Laboratory mice (C57BL6J) were obtained by housing a female and male pair overnight. The following morning pairs were separated and mid-day was considered embryonic day 0.5 (E0.5). Pregnancy was identified by body weight gain and physical appearance. At E12.5 pregnant dams received an intraperitoneal (IP) injection of either 20 mg/kg Poly I:C (catalog #P9852, Sigma-Aldrich, St. Louis, MO, USA) or vehicle (sterile phosphate buffered saline, PBS). The dosing of poly I:C and its route of administration were as in previously published studies (Smith et al., 2006; Choi et al., 2016). Dams were monitored for parturition. Male offspring of these mice (1 – 5 mice per litter) were used in our experiments. On postnatal day 9

JNeurosci Accepted Manuscript

(PND9), pups received a subcutaneous (SC) injection of 10 mg/kg LPS from *Escherichia coli* 0111:B4 (catalog #L3024, Sigma-Aldrich, St. Louis, MO, USA) or vehicle (endotoxin-free saline). The optimal dose of LPS and an efficient route of its administration were determined empirically in control studies. P9 in rodents approximately corresponds to 39-40-week human gestation (term infant; Semple et al., 2013; Custodio et al., 2017). Thus, we used the regimen providing bacterial challenge at P9 to mimic the environmental challenges which human newborns could meet very early postnatally.

Microglia immunohistochemistry and quantitative analysis. To confirm the presence of treatment-induced inflammatory responses in the brain, we examined brain microglia. Mice were deeply anesthetized with pentobarbital and transcardially perfused with phosphate buffered saline, followed by 4% paraformaldehyde. Brains were dissected, post-fixed in 4% paraformaldehyde overnight at 4°C, equilibrated to 30% sucrose, and then cryosectioned. Sections (30 µm) containing the BLA were permeabilized with 0.3% Triton X-100, blocked with 1% bovine serum albumin and 2% normal donkey serum, and then incubated with 1:400 rabbit anti-IBA-1 antibody (019-19471, Wako Chemicals, Osaka, Japan) overnight at 4°C. After rinses, sections were incubated in 1:200 anti-rabbit AlexaFluor 488 antibody for 2 hours, stained with DAPI (0.5µg/ml), rinsed, and then mounted on slides. Images were obtained with a 40x objective using a confocal laser-scanning microscope (TCS SP8, Leica, Wetzler, Germany) of the identical portion of the BLA. 5 µm z-stacks were obtained at Nyquist-derived optimal section thickness. All images were acquired under identical settings and parameters,

JNeurosci Accepted Manuscript

and then exported to ImageJ software (NIH) for analysis. Maximum projections were made and the total threshold signal per unit area, cell count, soma size, or ramifications of each image were quantified by semi-autonomous methods or by using a blinded scorer in ImageJ. The co-localization of DAPI and IBA-1 immunoreactivity was used to identify individual cells.

Behavioral tests. Effects of MIA or PIA alone on ASD-like behaviors have been reported (Smith et al., 2007; Custódio et al., 2017). To confirm treatment-induced changes in behavior, we used the open field to quantify anxiety-like responses, considering that anxiety is frequently co-morbid with ASD. Mice were placed in the corner of a brightly lit open field (44 cm x 44 cm x 30 cm) and allowed to freely explore for 10 minutes while being video recorded. The percentage of time the mouse spent in the center of the open field and total distance travel was analyzed using Ethovision-XT (Noldus Information Technology, Wageningen, the Netherlands). The social interaction test (Golden et al., 2011; Bagot et al., 2015) consisted of two separate 3-minute sessions. The first session consisted a mouse being placed in a chamber (44 cm x 44 cm x 30 cm) that contained an empty metal wire cage (10 cm x 8 cm x 6 cm) at the other end of the arena. In the second session an age-matched and sex-matched novel conspecific was placed in the metal cage, preventing direct physical contact. The duration of time in the interaction zone was calculated for both the empty cage and conspecific sessions using automated tracking software (Noldus Ethovision-XT 7.0). Data is presented as the social interaction ratio (mouse/empty interaction zone time) normalized to the Veh_Veh group.

JNeurosci Accepted Manuscript

202

203 *Viral constructs.* We used adeno-associated virus (AAV) carrying channelrhodopsin-
204 2(H143R)-eYFP under control of CaMKIIα promoter to investigate functional
205 connectivity in the mPFC-AMG circuits. Vectors were purchased from the viral vector
206 core facility at the University of North Carolina, and the titers were ~10.0 x 10^{12}
207 particles/ml.

208

209 *Stereotaxic surgery and viral injections.* Surgeries were performed by using medical
210 and laboratory aseptic techniques. Male offspring of immunoactivated mice (8-10
211 weeks old) were anesthetized with a mixture of ketamine and xylazine (160 mg/kg and
212 12 mg/kg body weight, respectively). The surgical procedures and viral injections were
213 performed as previously described (Cho et al., 2013). Briefly, bilateral craniotomy was
214 made to target the prelimbic cortex (PL) of the medial prefrontal cortex (mPFC) using
215 the stereotaxic coordinates: 1.8 mm rostral to Bregma, ± 0.4 mm lateral to midline, and
216 1.8 mm ventral to the skull surface (Franklin and Paxinos, 2007). The AAV vector
217 carrying channelrhodopsin-2(H143R)-eYFP was injected bilaterally into PL at a rate of
218 0.1 µl/minute under control of the syringe pump (Stoelting Co.). Mice were given 0.1 ml
219 ketoprofen (SC) (Boehringer Ingelheim) to reduce pain. After surgery, mice were single
220 housed for 8 weeks before behavioral or *ex vivo* electrophysiological experiments.

221

222 *Ex vivo electrophysiology and photostimulation.* After cervical dislocation and
223 decapitation, brains were removed and coronal slices (300 µm) containing the mPFC or
224 the AMG were obtained using a vibratome in cold cutting solution containing: 252 mM

JNeurosci Accepted Manuscript

sucrose, 1.0 mM $CaCl_2$, 5.0 mM $MgCl_2$, 2.5 KCl, 1.25 mM NaH_2PO_4, 26 mM NaHCO3, 10 mM glucose and equilibrated with 95% O_2 and 5% CO_2. Slices were then incubated in oxygenated artificial cerebrospinal fluid (ACSF) containing: 125 mM NaCl, 2.5 mM KCl, 2.5 mM $CaCl_2$, 1.0 mM $MgSO_4$, 1.25 mM NaH_2PO_4, 26 mM $NaHCO_3$ and 10 mM glucose at room temperature for at least one hour before electrophysiological recordings. The subnuclei of the AMG were visualized under a Zeiss microscope coupled with an IR-camera (Hamamatsu, Japan) and defined based on the structural landmarks of the internal capsule (ic) and the external capsule (ec). Whole-cell recording were obtained from neurons in the BLA with patch electrodes (3-5 MΩ resistance) containing: 130 mM Cs-methane-sulfonate, 5.0 mM KCl, 2.5 mM NaCl, 1.0 mM $MgCl_2$, 10 mM BAPTA, 10 mM HEPES, 2 mM MgATP, and 0.1 mM NaGTP (adjusted to pH 7.2 with KOH). Qx-314 (5 mM) and spermine (0.5 mM) were added in the internal solution before the recordings. To assay membrane properties and record photostimulation-induced action potentials in the mPFC (Fig. 2*D*), 130 mM K-gluconate was used instead of Cs-methane-sulfonate in the pipette solution. Neurobiotin (0.2%, Vector Labs) was added into the internal pipette solution to locate the recorded neurons in the the amygdala. Synaptic responses were induced by photostimulation of ChR2-expressing mPFC projecting fibers in the BLA through a 40x water-immersion objective lens (Carl Zeiss microscope) with a LED light source (excitation wavelength: 470 nm, 1 ms in duration, Thorlabs). All whole-cell recordings were performed at 30-32°C in the external medium. Current were filtered at 1 kHz and digitized at 5 kHz. After recordings, slices were placed in PBS containing 4% paraformaldehyde and kept in a refrigerator until histological processing.

JNeurosci Accepted Manuscript

To minimize the variability in photostimulation-induced synaptic responses between experimental groups, the volume of ChR2-encoding virus infused in the mPFC, coordinates of the PL and the expression time of ChR2 in the brain were kept constant throughout the study. Before the recordings, the extent and intensity of ChR2-eYFP expression at the injection site in acute slices containing the mPFC and ChR2-expressing fibers in the AMG (projection site) were evaluated under low (10x) magnification. To assay the effects of immunoactivation on functional expression of ChR2 in the brain, the amplitude of photostimulation-induced currents and the reliability of photostimulation-induced action potentials were examined in pyramidal neurons in layer V at the ChR2 injection site in the PL (Fig. 2*C,D*).

Pharmacological reagents used in the electrophysiological experiments, which included 2,3-Dioxo-6-nitro-1,2,3,4-tetrahydrobenzo[*f*]quinoxaline-7-sulfonamide (NBQX) disodium salt, D-(-)-2-amino-5-phosphonopentanoic acid (D-AP5), *N*-(2,6 dimethylphenylcarbamoylmethyl)triethylammonium (QX 314) chloride, (-)-bicuculline methobromide (from R&D Systems), and spermine tetrahydrochloride (from Sigma-Aldrich), were prepared as stock solutions in water at 1000- to 5000-fold concentrations and stored at -20°C.

Histology. Brain slices were washed in PBS (3 X 15 min) and incubated in 0.1% Triton PBS containing neurotracer fluorescent Nissl stain (diluted 40X, Molecular Probes) for 1 hr at room temperature, and then re-washed in PBS (3 X 20 min). Sections containing

JNeurosci Accepted Manuscript

neurobiotin loaded cells were incubated in 0.1% Triton PBS containing Streptavidin Alexa 568 conjugate (20 µg/ml, Molecular Probes) for 2 hr at room temperature, and then washed in PBS (3 X 20 min). Finally, sections were mounted on the gelatinized slides, dehydrated and coversliped. Vectashield mounting medium (Vector Laboratory) was applied to slices to prevent fluorescence fading. Viral vector infusion sites were examined under Leica TCS SP8 confocal microscope (Leica) or Zeiss Axioskop 2 fluorescent microscope (Carl Zeiss). Mice in which the injection missed the target (PL mPFC) were excluded from the analysis.

Analysis of mPFC projection patterns in the amygdala. To detect the effect of immunoactivation on mPFC projection patterns in different subnuclei of the AMG, the fluorescence intensity of ChR2-eYFP-expressing fibers within the subregion were quantitatively analyzed. Confocal fluorescent images were acquired using a Leica TCS SP8 confocal microscope (Leica) using a 10/0.40 NA objective lens. The settings for aperture gain, laser intensity and offset were optimized initially and then kept constant throughout the acquisition of images from all mice used for the analysis. Confocal z-stack images of ChR2-eYFP-expressing fibers in the amygdala contained 6-12 images which were captured 5 µm apart. The boundary of the subnuclei of the amygdala was defined based on landmark structures (internal and external capsules) and cellular morphology (Sah et al., 2003) revealed by fluorescent Nissl (and DAPI) counterstain. The fluorescence intensity on a single focal plane in the channel for ChR2-eYFP was measured using ImageJ (1.51f, National Institutes of Health, USA).

JNeurosci Accepted Manuscript

294 *Sholl analysis.* To detect the effect of immune activation on neuronal structure, we
295 reconstructed 32 neurobiotin-filled BLA neurons from all four experimental groups (8
296 neurons per group). The recorded and subsequently reconstructed cells were identified
297 as neurons based on their accommodating firing patterns (Tsvetkov et al., 2002).
298 Neurobiotin (6.0 mM) was added to the intrapipette solution. Stained neurons were
299 scanned with a Leica confocal microscope under 40x/1.30 NA objective lens. Confocal
300 z-stack images were processed using ImageJ and then reconstructed in the
301 NeuronStudio program (Version 0.9.92). As the program automatically determines the
302 3D position and branch diameter based on the imaging data, we used the manual
303 tracing tool to trace each branch analyzed. Specifically, we were starting the manual
304 tracing from the beginning of each primary dendrite, and were moving one node at a
305 time to form an entire path along a branch in the 2D or 3D window. The image of a
306 reconstructed neuron in Fig. 5*A* was generated with Neurolucida 360 (MBF Bioscience).
307 The dendritic length, dendritic surface area and the number of branch points were
308 measured using Sholl analysis (Sholl, 1953). Soma size was estimated by its largest
309 projection area of stack images, measured in ImageJ.
310
311 *Experimental design and statistical analysis.* Mice were randomly assigned to
312 experimental groups. In electrophysiological experiments, one neuron was recorded
313 per a slice. The numbers of mice and recorded neurons used for the analysis in
314 different experiments are indicated in the figure legends. Data are reported as means ±
315 the standard error of the mean (SEM). The experiments were conducted using a 2x2
316 factorial design (Fig. 1*A*), and results were analyzed with two-way or three-way ANOVA

JNeurosci Accepted Manuscript

317 when appropriate to assess main effects of either Poly I:C or LPS as well as of a third
318 factor when it was present (such as light power density, stimulation frequency, Bregma
319 plane, or distance from soma), and interaction effects, followed by post-hoc *Bonferroni's*
320 simultaneous multiple comparisons of each treatment group to Veh_Veh. When
321 appropriate, *Student's* two-tailed paired *t*-test was used. Statistical analysis was
322 performed with SigmaPlot 13.0 or Minitab 16. The results of the statistical analysis are
323 presented in the text or in the figure legends.
324
325 **RESULTS**
326 **Immune activation results in alterations of microglia in the BLA and leads to ASD-**
327 **linked behavioral impairments**
328 To investigate whether *in utero* and/or early life neuroinflammation could alter the signal
329 flow in the mPFC-AMG circuits and produce ASD-relevant behavioral dysfunction, we
330 administered either Poly I:C (20 mg/kg, IP) or vehicle (PBS) to pregnant female
331 C57BL/6J mice on day 12.5 of pregnancy (as in Smith et al., 2007). Subsequently,
332 male offspring from both groups (Poly I:C or vehicle-injected mothers) were injected
333 either with LPS (10 mg/kg; Poly I:C_LPS and Veh_LPS groups) or vehicle on postnatal
334 day 9.5 (PND9; Poly I:C_Veh and Veh_Veh groups) (Fig. 1*A*). Poly I:C binds to TLR3,
335 triggering production of type I interferons, whereas LPS activates TLR4 resulting in
336 release of TNF-α from macrophages (reviewed in Lombardo et al., 2017). Notably, Poly
337 I:C-induced neuroinflammation in pregnant mice is associated with activation of cytokine
338 signaling mediated by interleukin-6, capable of passing from a pregnant female through
339 the placenta to the fetal brain (Lombardo et al., 2017). Since it has been shown

JNeurosci Accepted Manuscript

previously that Poly I:C-induced MIA leads to lasting alterations of microglia in the offspring mice exhibiting characteristics of the microglial hyperactive state (Krstic et al., 2012; Knuesel et al., 2014), we performed immunostaining for a microglial marker, Ionized calcium binding adaptor molecule 1 (IBA-1), in 13-week-old offspring mice. In our analysis, we focused on the BLA, where prefrontal projection fibers were predominantly found (see below). We found that both the number of IBA-1 positive cells and the intensity of IBA-1 (Fig. 1*B*,*C*) staining (immunoreactivity, IR) were increased in the offspring groups receiving the postnatal LPS injections, indicating an activation of microglia approximately 12 weeks after the LPS injection at PND9 (Fig. 1*C*, left: two-way ANOVA, Poly I:C, $F_{(1,18)} = 0.356$, $p = 0.558$; LPS, $F_{(1,18)} = 25.821$, $p < 0.001$; interaction, $F_{(1,18)} = 0.241$, $p = 0.629$; post-hoc *Bonferroni's* test: $P < 0.009$ for Veh_Veh versus Veh_LPS and $P = 003$ for Veh_Veh versus Poly I:C_LPS; Fig. 1*C*, right: two-way ANOVA, Poly I:C, $F_{(1,18)} = 0.538$, $p = 0.473$; LPS, $F_{(1,18)} = 17.538$, $p < 0.001$; interaction, $F_{(1,18)} = 0.108$, $p = 0.747$; post-hoc *Bonferroni's* test: $p < 0.05$ for Veh_Veh versus Veh_LPS or for Veh_Veh versus Poly I:C_LPS). There were no significant differences in microglial soma size or the number of microglial ramifications between experimental groups (Fig. 1*D*; soma size: two-way ANOVA, Poly I:C, $F_{(1,234)} = 3.334$, $p = 0.069$; LPS, $F_{(1,234)} = 0.462$, $p = 0.497$; interaction, $F_{(1,234)} = 2.339$, $p = 0.128$; number of ramifications: two-way ANOVA, Poly I:C, $F_{(1,234)} = 3.238$, $p = 0.073$; LPS, $F_{(1,234)} = 1.268$, $p = 0.261$; interaction, $F_{(1,234)} = 0.019$, $p = 0.892$).

Accompanying these inflammatory markers, there were group differences in anxiety and social behavior. Thus, mice in the Veh_LPS group exhibited increased anxiety-like

JNeurosci Accepted Manuscript

behavior in the open field test (Briton et al., 1981; File et al., 1985; Riccio et al., 2009; Riccio et al., 2014). Specifically, these mice spent less time in the center of the open field compared to the Veh_Veh group (Fig. 1*E*), which is commonly interpreted as an increased anxiety-like behavioral response (Lezak et al. 2017). This effect was not due to decreased locomotor activity because animals in the Veh_LPS group did not differ from mice in the control Veh_Veh group in the total distance traveled (Fig. 1*E*). Notably, mice in the Poly I:C_LPS group also showed increased anxiety-like responses (Fig. 1*E*; time in center (%): two-way ANOVA, Poly I:C, $F_{(1,78)} = 2.291$, $p = 0.134$; LPS, $F_{(1,78)} = 17.052$, $p < 0.001$; interaction, $F_{(1,78)} = 0.008$, $p = 0.928$; post-hoc *Bonferroni's* test: $p < 0.05$ for Veh_Veh versus Veh_LPS and $p < 0.001$ for Veh_Veh versus Poly I:C_LPS). In this experimental group, the total distance traveled was increased compared to Veh_Veh control mice (Fig. 1*E*, distance traveled: two-way ANOVA, Poly I:C, $F_{(1,78)} = 4.293$, $p = 0.042$; LPS, $F_{(1,78)} = 3.275$, $p = 0.074$; interaction, $F_{(1,78)} = 0.014$, $p = 0.906$; post-hoc *Bonferroni's* test: $p < 0.05$ for Veh_Veh versus Poly I:C_LPS). However, it is unlikely that slight increases in locomotor activity can explain the enhanced anxiogenesis in Poly I:C_LPS mice, as enhanced locomotion may slightly blunt anxiety-like responses rather than promote them due to the fact that more actively moving mice could randomly cross into the anxiogenic center more often. In agreement with the role of immune activation in the development of ASD-linked behavioral dysfunctions, we also found that social interactions were diminished in our experimental groups. Thus, mice in both Veh_LPS and Poly I:C_LPS groups spent less time in the interaction zone with the novel conspecific mouse (Fig. 1*F*, left, two-way ANOVA, Poly I:C, $F_{(1,54)} = 2.397$, $p = 0.127$; LPS, $F_{(1,54)} = 10.157$, $p = 0.002$; interaction, $F_{(1,54)} = 1.923$, $p = 0.171$; post-hoc

JNeurosci Accepted Manuscript

386 *Bonferroni's* test: $p = 0.014$ for Veh_Veh group versus Veh_LPS group and $p = 0.004$
387 for Veh_Veh versus Poly I:C_LPS). However, there was no treatment effect on the
388 distance traveled during the social interaction test (Fig. 1*F*, right, two-way ANOVA, Poly
389 I:C, $F_{(1,54)} = 0.161$, $p = 0.69$; LPS, $F_{(1,54)} = 0.313$, $p = 0.578$; interaction, $F_{(1,54)} = 0.109$, p
390 $= 0.743$).
391
392 Together, these findings indicate that perinatal immune activation can trigger long-
393 lasting alterations in brain and behavior.
394
395 **Projection-specific optogenetic targeting of mPFC-amygdala circuits**
396 To target neuronal projections from mPFC to AMG for the subsequent functional
397 analysis, we expressed channelrhodopsin2 (ChR2) in the mPFC by stereotaxically
398 injecting AAV5-CamKIIα-ChR2-eYFP) in mice from all four experimental groups (Fig.
399 2*A*). Eight weeks after gene transfer, eYFP-tagged ChR2 was densely expressed at the
400 injection site (Fig. 2*B*). Although the tip of an injection pipette was placed within the
401 prelimbic mPFC (PL), the ChR2-eYFP-mediated green fluorescent signal was also
402 observed in the infralimbic mPFC (IL), suggesting that both IL- and PL-originating
403 projections were activated in these experiments. Notably, we found previously that the
404 IL and PL projection patterns to the AMG are virtually identical (Cho et al., 2013). By
405 performing whole-cell recordings from virally transduced neurons, we confirmed the
406 functionality of ChR2 expression at the mPFC injection site. Delivery of prolonged
407 pulses of blue light (470 nm) of increasing intensity triggered inward currents with
408 transient and sustained components in recorded neurons under voltage-clamp

JNeurosci Accepted Manuscript

409 recording conditions at a holding potential of -80 mV (Fig. 2*C*). We did not observe
410 differences in the peak photocurrent amplitude between the groups, indicating that
411 neither MIA nor PIA had effects on ChR2 expression in the mPFC (Fig. 2*C*; three-way
412 ANOVA (Poly I:C x LPS x light power density); Poly I:C, $F_{(1,474)} = 0.199$, $p = 0.651$; LPS,
413 $F_{(1,474)} = 0.003$, $p = 0.986$; interaction, $F_{(5,474)} = 0.227$, $p = 0.951$). In current-clamp
414 recordings, short (5-ms-long) pulses of blue light evoked action potential (AP) firing, with
415 spikes reliably following higher frequencies of photostimulation (up to 40 Hz) (Fig. 2*D*).
416 Consistent with the lack of the effect of neuroinflammation on the ability of ChR2 to
417 drive neuronal spiking, the input-output curves for the probability of AP firing in
418 response to trains of photostimuli of increasing frequency did not differ between the
419 experimental groups (Fig. 2*D*; three way-way ANOVA (Poly I:C x LPS x stimulation
420 frequency); Poly I:C, $F_{(1,103)} = 0.0003$, $p = 0.996$; LPS, $F_{(1,103)} = 2.425$, $p = 0.122$;
421 interaction, $F_{(3,103)} = 0.967$, $p = 0.411$).
422
423 Consistent with previous reports (Cho et al., 2013), the ChR2-eYFP-expressing fibers
424 arising from the virally-transduced neurons in the mPFC were found predominantly in
425 the BLA (Fig. 3). We confirmed that mPFC projections form functional synapses on
426 neurons in the BLA by performing whole-cell recordings from these cells and triggering
427 the excitatory postsynaptic currents (EPSCs) in them in voltage-clamp mode at -80 mV
428 by 5-ms pulses of blue light (Fig. 3*A*). The EPSCs at the mPFC-BLA synapses were
429 glutamatergic, as indicated by their sensitivity to NBQX (10 μM), an α-amino-3-hydroxy-
430 5-methyl-4-isoxazolepropionic acid (AMPA)/kainate receptor antagonist (Fig. 3*A*).
431 Synaptic responses were suppressed by tetrodotoxin (TTX, 1 μM), a sodium channel

JNeurosci Accepted Manuscript

blocker, providing evidence that they were mediated by presynaptic action potential firing (as in Cho et al., 2013). Under these recording conditions, the glutamatergic EPSCs in mPFC-AMG projections are monosynaptic, as they could be rescued by an exogenously-applied blocker of voltage-gated K+ channels, 4-aminopyridine (4-AP) when the EPSCs were blocked by TTX (Petreanu et al., 2009; Cho et al., 2013; Fig. 3*C,D*). In agreement with our previous report (Cho et al., 2013), photostimulation of mPFC fibers induced EPSCs in all recorded BLA neurons (140 neurons) and in most intercalated cells (ITCs; 81.8%, 27 out of 33 neurons (Fig. 3*B*) (but see Strobel et al., 2015, and Luchkina and Bolshakov, 2017 for discussion of possible reasons of why monosynaptic mPFC inputs to ITCs were not detected in Strobel et al., 2015). ITCs possess very high membrane resistance (>1.0 GOhm) and thus could be reliably identified in slice recordings (Cho et al., 2013). The synaptic connectivity between the mPFC and lateral nucleus of the amygdala (LA) or lateral subnucleus of the central amygdala (CeL) was very sparse (in LA, 25%, 7 out of 28 neurons exhibited synaptic responses; in CeL, 20%, 7 out of 35 neurons). Notably, we found that neither MIA, PIA nor MIA + PIA affected the fraction of BLA neurons or ITCs (relative to the total number of recorded cells) in which photostimulation-induced EPSCs could be observed at the maximum light intensity of 10.5 mW/mm^2 (Fig. 3*B*).

We also compared the fluorescence intensity of ChR2-eYFP-expressing mPFC projections in various parts of the AMG in brain slices between all experimental groups along the rostral-caudal axis at three different Bregma levels (Fig. 3*E*,*F*; see Materials and Methods for the quantification details). Consistent with the lack of a treatment

JNeurosci Accepted Manuscript

455 effect on the functional synaptic connectivity at mPFC projections to LA and CeL, the
456 mean density of ChR2-eYFP fluorescence in these two AMG subnuclei remained
457 unchanged (Fig. 3*H,I*; LA: three-way ANOVA (Poly I:C x LPS x Bregma plane); Poly I:C,
458 $F_{(1,54)}$ = 0.037, p = 0.849; LPS, $F_{(1,54)}$ = 0.012, p = 0.914; interaction, $F_{(2,53)}$ = 0.128, p =
459 0.88; CeL: three-way ANOVA (Poly I:C x LPS x Bregma plane), Poly I:C, $F_{(1,53)}$ = 0.138,
460 p = 0.712; LPS, $F_{(1,53)}$ = 1.321, p = 0.256; interaction, $F_{(2,53)}$ = 0.137, p = 0.872).
461 However, the fluorescence density was significantly enhanced in the BLA of mice from
462 the Poly I:C_LPS group (Fig. 3*G*; BLA: three-way ANOVA (Poly I:C x LPS x Bregma
463 plane); Poly I:C, $F_{(1,53)}$ = 3.57, p = 0.064; LPS, $F_{(1,53)}$ = 9.178, p = 0.004; interaction,
464 $F_{(2,53)}$ = 0.320, p = 0.728; post-hoc Bonferonni's simultaneous multiple comparisons: p =
465 0.003 for Veh_Veh versus Poly I:C_LPS), suggesting that the innervation of BLA by
466 mPFC fibers might be increased in the MIA+PIA group.
467
468 **Prenatal MIA but not PIA is associated with synaptic strengthening at**
469 **glutamatergic projections from mPFC to BLA**
470 We examined the effects of immunoactivation on synaptic transmission in the mPFC-
471 BLA projections by performing whole-cell patch-clamp recordings of the light-induced
472 EPSCs in BLA neurons in brain slices obtained from all experimental treatment groups
473 (Veh-Veh, Poly I:C-Veh, Veh_LPS or Poly I:C_LPS; see above for details) (Fig. 4*A-C*).
474 EPSCs were recorded in voltage-clamp mode at a holding potential of -80 mV. There
475 were no treatment-induced alterations in the passive membrane properties of BLA
476 neurons (Table 1). However, we found that synaptic strength, as quantified by input-
477 output curves for EPSCs induced by the 1-ms pulses of blue light, was significantly

JNeurosci Accepted Manuscript

478 increased in both Poly I:C_Veh and Poly I:C_LPS groups compared to control Veh-Veh
479 mice (Fig. 4*C*,*D*; three-way ANOVA (Poly I:C x LPS x light power density), Poly I:C,
480 $F_{(1,798)}$ = 54.262, p < 0.001; LPS, $F_{(1,798)}$ = 0.049, p = 0.825; interaction, $F_{(5,798)}$ = 0.305, p
481 = 0.91; post-hoc *Bonferroni's* simultaneous multiple comparisons: p = 0.003 for
482 Veh_Veh versus Poly I:C_Veh and p < 0.001 for Veh_Veh versus Poly I:C_LPS). The
483 lack of a detectable effect in these experiments on the magnitude of mPFC-BLA EPSCs
484 in the Veh_LPS group indicates that the observed increases in the efficacy of
485 glutamatergic neurotransmission in mPFC-BLA projections could be specifically
486 attributed to MIA.
487
488 We next explored synaptic expression mechanisms of MIA-triggered synaptic
489 potentiation in mPFC-BLA projections. The observed synaptic strengthening could be
490 due either to enhanced probability of neurotransmitter release (*P*r) or increased
491 responsiveness to single quanta of glutamate, or both, as well as due to increases in
492 the number of sites of synaptic transmission (Zucker and Regehr, 2002; Tsvetkov et al.,
493 2002; Goussakov et al., 2006; Cho et al., 2013). We found that the magnitude of the
494 paired-pulse ratio (PPR) at the mPFC-BLA synapses, a commonly used measure of
495 presynaptic function (*P*r, specifically), was identical in slices from all experimental
496 groups, indicating that *P*r at prefrontal glutamatergic inputs to BLA remained unaffected
497 by MIA, PIA or MIA+PIA (Fig. 4*E*,*F*; two-way ANOVA, Poly I:C, $F_{(1,89)}$ = 0.99, p = 0.321;
498 LPS, $F_{(1,89)}$ = 0.483, p = 0.489; interaction, $F_{(1,89)}$ = 0.04, p = 0.852). To address the
499 possibility that immunoactivation could be associated with postsynaptic modifications at
500 glutamatergic inputs to BLA neurons, we recorded and analyzed spontaneous EPSCs

JNeurosci Accepted Manuscript

(sEPSCs), which reflect synaptic responses to single quanta of glutamate (Li et al., 2013) (Fig. 4*G-I*). The sEPSCs were recorded at a holding potential of -80 mV in the presence of bicuculline (30 μM). Consistent with the potentiating effect of MIA on evoked, light-induced synaptic responses, the amplitude of sEPSPs was enhanced in Poly I:C_Veh and Poly I:C_LPS groups relative to control Veh-Veh mice (Fig. 4*J*; two-way ANOVA, Poly I:C, $F_{(1,32)} = 17.523$, $p < 0.001$; LPS, $F_{(1,32)} = 0.292$, $p = 0.593$; interaction, $F_{(1,32)} = 0.251$, $p = 0.62$; post-hoc *Bonferroni's* test: $p = 0.007$ for Veh_Veh versus Poly I:C_Veh and $p = 0.002$ for Veh_Veh versus Poly I:C_LPS). However, the frequency of sEPSC, reflecting presynaptic function, was not altered (Fig. 4*K*; two-way ANOVA, Poly I:C, $F_{(1,32)} = 0.02$, $p = 0.887$; LPS, $F_{(1,32)} = 0.361$, $p = 0.552$; interaction, $F_{(1,32)} = 0.187$, $p = 0.669$). Together, these results suggest that potentiation of glutamatergic synaptic transmission in mPFC-BLA projections in Poly I:C_Veh and Poly I:C_LPS groups may be postsynaptically regulated.

Notably, Sholl analyses of neuronal structure in neurobiotin-filled BLA principal neurons in fixed tissue sections showed that immune activation was associated with morphological changes. Thus, the averaged soma size (area) was increased in Poly I:C_LPS-treated mice (Fig. 5*A,B*; soma size: two-way ANOVA, Poly I:C, $F_{(1,28)} = 2.553$, $p = 0.121$; LPS, $F_{(1,28)} = 11.417$, $p = 0.002$; interaction, $F_{(1,28)} = 0.085$, $p = 0.773$, post-hoc *Bonferroni's* test: $p = 0.005$ for Veh_Veh vs Poly IC_LPS). We detected the main effect of LPS treatment on the number of primary dendrites (Fig. 1*C*; two-way ANOVA, Poly I:C, $F_{(1,28)} = 0.914$, $p = 0.347$; LPS, $F_{(1,28)} = 5.264$, $p = 0.029$; interaction, $F_{(1,28)} = 0.91$, $p = 0.347$). However, post-hoc *Bonferroni's* test did not reveal statistically

JNeurosci Accepted Manuscript

524 significant differences between Veh_Veh and Poly IC_LPS groups ($F_{(3,28)}$ = 2.364, p =
525 0.092). The dendritic surface area and averaged dendritic diameter were also
526 enhanced in Veh_LPS and Poly I:C_LPS groups (Fig. 5*E,G*), as well as the dendritic
527 length in the Veh-LPS group (Fig. 5*D*), whereas the number of branch points was
528 unaffected by immune activation (Fig. 5*C,F*).
529
530 **PIA selectively decreases feed-forward GABAergic inhibition in mPFC-BLA**
531 **projections**
532 Excitatory neurotransmission in the BLA is under strong inhibitory control by local circuit
533 GABA-releasing interneurons (Ehrlich et al., 2009). Specifically, BLA interneurons
534 receive direct glutamatergic inputs from the mPFC, and when interneurons are driven
535 above the AP firing threshold, this results in feed-forward inhibition of BLA principal
536 neurons (Fig. 6*A*; Cho et al., 2013). We explored whether neuronal immunoactivation
537 could affect the efficacy of feed-forward inhibition in mPFC-BLA projections, thereby
538 modifying the firing output of BLA neurons. Consistent with previous reports, activation
539 of mPFC projections to the BLA by pulses of blue light resulted in monosynaptic (see
540 above) glutamatergic EPSCs in recorded neurons which were followed by $GABA_A$
541 receptor-mediated inhibitory postsynaptic currents (IPSCs). To record the excitatory
542 and inhibitory responses from the same neurons in isolation, we evoked the EPSCs at a
543 holding potential of -80 mV (close to the reversal potential for chloride-mediated
544 GABAergic IPSCs and the IPSCs at 0 mV (the reversal potential for AMPA receptor
545 EPSCs) (as in Cho et al., 2013) (Fig. 6*B*). Synaptic latencies of IPSCs were ~2 times
546 longer than those of the EPSCs, consistent with the disynaptic nature of inhibitory

JNeurosci Accepted Manuscript

responses (Fig. 5*B*; Student's two-tailed paired *t*-test, $t_{(14)} = 5.296$, $p < 0.001$ for the comparison between synaptic latencies of EPSCs and IPSCs). The IPSCs at 0 mV were completely blocked by bicuculline (30 μM), confirming that IPSCs were mediated by activation of $GABA_A$ receptors and were not contaminated by EPSCs at this holding potential (Fig. 6*C*). Conversely, the EPSCs at -80 mV were suppressed by AMPA/kainate and N-methyl-D-aspartate (NMDA) receptor antagonists (10 μM NBQX and 50 μM D-AP5, respectively), when the antagonists were applied together (Fig. 6*D*). $GABA_A$R-IPSCs were also completely blocked by the application of NBQX and D-AP5, confirming that they were disynaptic, mediating feed-forward inhibition of BLA neurons (Fig. 6*D*).

To examine the effects of immunoactivation on feed-forward inhibition in mPFC-BLA projections, we first recorded photostimulation-induced glutamatergic EPSCs at -80 mV and then GABAergic IPSCs at 0 mV (see above) from the same neurons in the BLA (Fig. 6*E*) in control and treated mice, and calculated IPSC/EPSC amplitude ratios in all experimental groups. We found that these ratios were significantly reduced in slices from Veh_LPS and Poly I:C_LPS groups compared to control Veh_Veh animals (Fig. 6*F*; two-way ANOVA, Poly I:C, $F_{(1,67)} = 0.004$, $p = 0.95$; LPS, $F_{(1,67)} = 14.598$, $p < 0.001$; interaction, $F_{(1,67)} = 0.148$, $p = 0.702$; post-hoc *Bonferroni's* test: $p = 0.044$ for Veh_Veh versus Veh_LPS and $p = 0.027$ for Veh_Veh versus Poly I:C_LPS). However, IPSC/EPSC amplitude ratios were not altered in the Poly I:C_Veh group. Notably, neither MIA, PIA nor MIA+PIA had effects on the latencies of synaptic responses in mPFC inputs to the BLA (Fig. 6*G*; EPSC latencies: two-way ANOVA, Poly I:C, $F_{(1,67)} =$

JNeurosci Accepted Manuscript

570 1.733, p = 0.193; LPS, $F_{(1,67)}$ = 1.245, p = 0.269; interaction, $F_{(1,67)}$ = 1.522, p = 0.222;
571 IPSC latencies: two-way ANOVA, Poly I:C, $F_{(1,67)}$ = 2.538, p = 0.116; LPS, $F_{(1,67)}$ = 0.402,
572 p = 0.528; interaction, $F_{(1,67)}$ = 0.519, p = 0.474). Considered together with the fact that
573 the efficacy of glutamatergic synaptic transmission was unaffected in Veh_LPS mice
574 (Fig. 4*C,D*), these findings suggest that PIA, but not MIA, led to decreased feed-forward
575 inhibition, thus shifting the balance between inhibition and excitation in mPFC-BLA
576 projections toward a greater functional efficiency of excitation. Therefore, it appears
577 that MIA and PIA may have distinct cellular targets in the BLA.
578
579 **Neuroinflammation-induced synaptic modifications in mPFC-BLA projections**
580 **lead to increased firing output of BLA neurons**
581 To explore the functional consequences of MIA-induced strengthening of glutamatergic
582 synapses and PIA-induced suppression of feed-forward GABAergic inhibitory responses
583 in prefrontal projections to the BLA, we tested the effects of immunoactivation on the
584 probability of synaptically-driven spiking at the studied pathways (Riccio et al., 2009;
585 Cho et al., 2012; Cho et al., 2013). We induced extracellular synaptically-triggered
586 spikes with photostimuli of increasing intensity (ranging from 0.5 to 10.2 mW/mm^2) and
587 recorded them in BLA neurons in a cell-attached patch configuration (Fig. 7*A,B*). Under
588 these recording conditions, we minimized the contribution of voltage errors, which might
589 be prominent for synaptic responses exceeding 1 nA in amplitude (see Fig. 4*C*), and
590 avoided the potential problems associated with prolonged whole-cell recordings, which
591 can disturb the intracellular milieu thus possibly affecting the properties of recorded
592 neurons (Cho et al., 2011). Notably, the probability of AP generation was dramatically

JNeurosci Accepted Manuscript

593 increased when the $GABA_A$ receptor antagonist bicuculline (30 μM) was added to the
594 external medium (Fig. 7*C,D*; two-way ANOVA, $F_{(1,84)} = 14.169$, $p < 0.001$), providing
595 evidence that synaptically-driven spike output of BLA neurons is under inhibitory control.
596 We then compared the average number of extracellular spikes triggered in BLA neurons
597 by single pulses of light of increasing intensity delivered to the ChR2-expressing mPFC
598 fibers. We found that the probability of neuronal firing induced by synaptic activation
599 was increased in slices from the Veh_LPS group only (relative to the control Veh_Veh
600 group) (Fig. 7*E*,*F*; three-way ANOVA (Poly I:C x LPS x light power density), Poly I:C,
601 $F_{(1,442)} = 23.474$, $p < 0.001$; LPS, $F_{(1,442)} = 34.994$, $p < 0.001$; interaction, $F_{(1,442)} = 1.027$,
602 $p = 0.401$; post-hoc *Bonferroni's* multiple comparisons: $p < 0.001$ for Veh_Veh versus
603 Veh_LPS, whereas there was no effect of the treatments on spike output of BLA
604 neurons in Poly I:C_Veh or Poly I:C_LPS groups.
605
606 Considered together, our findings provide evidence that neuroinflammation-associated
607 synaptic modifications are functionally relevant, modifying the signal flow in mPFC-BLA
608 circuits, and that the various manipulations (MIA, PIA, MIA+PIA) can be distinguished
609 from each other using our methodologies, enabling the development of a model that
610 depicts the specific effects of each process (Fig. 8).
611
612 **DISCUSSION**
613 Our studies provide evidence that MIA and PIA could have distinct cellular targets in the
614 brain. Specifically, our MIA regimen (prenatal PolyI:C) led to the strengthening of
615 monosynaptic glutamatergic inputs of the mPFC-arising afferents to principal neurons in

JNeurosci Accepted Manuscript

the BLA, whereas our PIA regimen (postnatal LPS) suppressed feed-forward $GABA_AR$-mediated inhibition of BLA neurons by local circuit interneurons. The resulting shift in the balance between excitation and inhibition in mPFC-BLA projections, enhancing the functional efficiency of excitatory prefrontal inputs, translated into the increased firing of BLA neurons. These physiological alterations were accompanied by increases in anxiety-like behavior and decreases in social interactions, in groups in which mice had received LPS treatment (Veh_LPS and Poly I:C_LPS). Conversely, systemic neuroinflammation has been shown previously to result in increased neuronal activity within the AMG, which was correlated with increases in anxiety-like behavior (Engler et al., 2011). The fact that all of the immune-activating treatments produced distinct physiological consequences, even in the absence of a significant change in behavior (e.g., Poly I:C_Veh mice), suggest a potentially higher sensitivity of the electrophysiological techniques in detecting effects that might be below the threshold for significantly altering behavioral endpoints.

Our results enable the development of a circuit model that captures the unique "physiological signature" of each treatment. Mechanistically, in the offspring of Poly I:C-treated dams (Poly I:C_Veh group), the efficacy of glutamatergic synaptic transmission in mPFC projections to both BLA principal neurons (PN) and BLA interneurons (IN) was proportionally increased (shown as thicker red lines in Fig. 8*B*), reflected in proportionally increased amplitudes of EPSCs and IPSCs. The proportionality of the effect of MIA on EPCS and IPSCs is supported by the finding that the IPSC/EPSC amplitude ratio in slices from these mice was unaffected relative to control Veh_Veh

JNeurosci Accepted Manuscript

mice. Consistent with this, the spike output of BLA neurons in response to activation of mPFC afferents remained unchanged. Postnatal immunoactivation alone (VEH_LPS group) did not affect synaptic efficacy at glutamatergic mPFC inputs to the BLA, but it was associated with decreases in the amplitude of feed-forward IN-mediated IPSCs (represented as a thinner blue line in the diagram in Fig. 8*C*). The resulting decreases in the IPSC/EPSC amplitude ratio led to the increased functional efficiency of neurotransmission in the mPFC-BLA projections, translating into the increased spike output of BLA PNs. In mice from the Poly I:C_LPS group, the BLA spike output appears to be determined by complex interactions between the effects of MIA (increased synaptic strength at both glutamatergic and GABAergic inputs to BLA PNs) and PIA-induced decreases in inhibition. Although the opposing effects of MIA and PIA on feed-forward inhibition partially compensate each other, the IPSC/EPSC amplitude ratio was still decreased relative to control animals (Fig. 8*D*). However, this shift toward a greater functional efficiency of excitation in the Poly I:C_LPS group was insufficient to affect the spike output of BLA neurons in mPFC-BLA projections. Regardless, each of the three treatments produces a unique signature that can be differentiated from the others.

Our finding that the altered signal flow in the mPFC-amygdala pathways may result in enhanced anxiety and decreased social interactions is consistent with previously published observations implicating both the mPFC (Elliott et al., 2016; Felix-Ortiz et al., 2016; Vila-Verde et al., 2016) and BLA complex (Sanders et al., 1995; Frankland et al., 1997; Perez de la Mora et al., 2006) in control of innate fear and anxiety responses. In addition, we recently reported evidence that, among other mechanisms, the activation of

JNeurosci Accepted Manuscript

662 the BLA complex mediates anxiogenesis (Riccio et al., 2014). Specifically, we found
663 that the knockdown of the Transient Receptor Potential Channel Subunit 4 (TRPC4)
664 subunit, abundantly expressed in brain areas controlling innate fear responses in the
665 normal mouse brain, in the lateral amygdala resulted in suppressed innate fear
666 responses as quantified with anxiety-probing behavioral tests. Our present results link
667 together these previously disparate observations, highlighting the role of mPFC-BLA
668 projections in control of anxiety-like behaviors, which are frequently co-morbid with ASD
669 (South et al., 2017). Considering that it has been shown that MIA alone and PIA alone
670 can each produce behavioral signs in mice that resemble the core features of ASDs
671 (e.g., aberrant social interactions, communication deficits, and increases in stereotyped
672 behaviors) (Smith et al., 2007; Custódio et al., 2017), our data raise the possibility that
673 mPFC-BLA functional interactions could be affected in humans with ASD.
674
675 It is important to emphasize that our studies characterize the effects of using Poly I:C as
676 the trigger for MIA and LPS as the trigger for PIA. We selected this order to
677 approximate the human condition, where postnatal bacterial infections (modeled by LPS)
678 are highly prevalent (Bilbo et al., 2009). In addition, this order of treatment matches well
679 with models that describe the putative time course of TLR3 (the receptor at which Poly
680 I:C acts) and TLR4 (the receptor at which LPS acts) expression (Barak et al., 2014).
681 Other permutations of this treatment regimen may yield different outcomes.
682
683 The mechanisms we describe here could contribute to the behavioral manifestations of
684 ASD, providing evidence that the development of ASD may implicate dysregulation of

JNeurosci Accepted Manuscript

685 the functional connectivity between distinct brain regions involved in control of specific
686 behavioral mechanisms (Markram and Markram, 2010; Monk et al., 2010; Rudie et al.,
687 2012). More generally, our work lends support to a theory that the development of ASD
688 may be associated with the excitation/inhibition imbalance in the brain leading to
689 increased excitability of relevant neural circuits (Hussman, 2001; Rubenstein and
690 Merzenich, 2003; Nelson and Valakh, 2015; Canetta et al., 2016; Lee et al., 2017).
691 Future studies will be needed to identify molecular pathways implicated in
692 neuroinflammation-induced synaptic changes in the mPFC-BLA circuits, and to
693 determine if there might be sex differences that contribute to the prevalence of
694 conditions such as ASD (Baron-Cohen et al., 2005; Werling and Geschwind, 2013).
695

696 **REFERENCES**

697 Abrahams BS, Geschwind DH (2008) Advances in autism genetics: on the threshold of
698 a new neurobiology. Nat Rev Genet 9:341-355.

699 Atladótir HO, Thorsen P, Østergaard L, Schendel DE, Lemcke S, Abdallah M, Parner
700 ET (2010) Maternal infection requiring hospitalization during pregnancy and autism
701 spectrum disorders. J Autism Dev Disord 40:1423-1430.

702 Bagot RC, Parise EM, Peña CJ, Zhang HX, Maze I, Chaudhury D, Persaud B, Cachope
703 R, Bolaños-Guzmán CA, Cheer JF, Deisseroth K,Han MH, Nestler EJ (2015) Ventral
704 hippocampal afferents to the nucleus accumbens regulate susceptibility to depression.
705 Nat Commun 6:7626.
706

707 Barak B, Feldman N, Okun E (2014) Toll-like receptors as developmental tools that
708 regulate neurogenesis during development: an update. Front Neurosci 8:272.
709

710 Baron-Cohen S, Knickmeyer RC, Belmonte MK (2005) Sex differences in the brain:
711 implications for explaining autism. Science 310:819-823.
712

713 Baron-Cohen S, Ring HA, Wheelwright S, Bullmore ET, Brammer MJ, Simmons A,
714 Williams SC (1999) Social intelligence in the normal and autistic brain: an fMRI study.
715 Eur J Neurosci 11:1891-1898.
716

JNeurosci Accepted Manuscript

717 Betancur C (2011) Etiological heterogeneity in autism spectrum disorders: more than
718 100 genetic and genomic disorders and still counting. Brain Res 1380:42-77.
719
720 Bilbo SD, Schwarz JM (2009) Early-Life Programming of Later-Life Brain and Behavior:
721 A Critical Role for the Immune System. Front Behav Neurosci 3:14.
722
723 Boyden ES, Zhang F, Bamberg E, Nagel G, Deisseroth K (2005) Millisecond-timescale,
724 genetically targeted optical control of neural activity. Nat Neurosci 8:1263-1268.
725
726 Britton DR, Britton KT (1981) A sensitive open field measure of anxiolytic drug activity.
727 Pharmacol Biochem Behav 15:577-582.
728
729 Canetta S, Bolkan S, Padilla-Coreano N, Song LJ, Sahn R, Harrison NL, Gordon JA,
730 Brown A, Kellendonk C (2016) Maternal immune activation leads to selective functional
731 deficits in offspring parvalbumin interneurons. Mol Psychiatry 21:956-68.

732 Cho JH, Bayazitov IT, Meloni EG, Myers KM, Carlezon WA Jr, Zakharenko SS,
733 Bolshakov VY (2011) Coactivation of thalamic and cortical pathways induces input
734 timing-dependent plasticity in amygdala. Nat Neurosci 15:113-122.
735
736 Cho JH, Zushida K, Shumyatsky GP, Carlezon WA Jr, Meloni EG, Bolshakov VY (2012)
737 Pituitary adenylate cyclase-activating polypeptide induces postsynaptically expressed
738 potentiation in the intra-amygdala circuit. J Neurosci 32:14165-14177.
739
740 Cho JH, Deisseroth K, Bolshakov VY (2013) Synaptic encoding of fear extinction in
741 mPFC-amygdala circuits. Neuron 80:1491-1507.
742
743 Choi GB, Yim YS, Wong H, Kim S, Kim H, Kim SV, Hoeffer CA, Littman DR, Huh JR
744 (2016) The maternal interleukin-17a pathway in mice promotes autism-like phenotypes
745 in offspring. Science 351:933-939

746 Custódio CS, Mello BSF, Filho AJMC, de Carvalho Lima CN, Cordeiro RC, Miyajima F,
747 Réus GZ, Vasconcelos SMM, Barichello T, Quevedo J, de Oliveira AC, de Lucena DF,
748 Macedo DS (2017) Neonatal immune challenge with lipopolysaccharide triggers long-
749 lasting sex- and age-related behavioral and immune/neurotrophic alterations in mice:
750 relevance to autism spectrum disorders. Mol Neurobiol 54:Epub ahead of print.

751 Ehrlich I, Humeau Y, Grenier F, Ciocchi S, Herry C, Lüthi A (2009) Amygdala inhibitory
752 circuits and the control of fear memory. Neuron 62:757-771.
753
754 Elliott E, Manashirov S, Zwang R, Gil S, Tsoory M, Shemesh Y, Chen A (2016) Dnmt3a
755 in the medial prefrontal cortex regulates anxiety-like behavior in adult mice. J Neurosci
756 36:730-740.
757

JNeurosci Accepted Manuscript

758 Engler H, Doenlen R, Engler A, Riether C, Prager G, Niemi MB, Pacheco-López G,
759 Krügel U, Schedlowski M (2011) Acute amygdaloid response to systemic inflammation.
760 Brain Behav Immun 25:1384-1392.
761
762 File SE (1985) What can be learned from the effects of benzodiazepines on exploratory
763 behavior? Neurosci Biobehav Rev 9:45-54.
764
765 Felix-Ortiz AC, Burgos-Robles A, Bhagat ND, Leppla CA, Tye KM (2016) Bidirectional
766 modulation of anxiety-related and social behaviors by amygdala projections to the
767 medial prefrontal cortex. Neuroscience 321: 197-209.
768
769 Frankland PW, Josselyn SA, Bradwejn J, Vaccarino FJ, Yeomans JS (1997) Activation
770 of amygdala cholecystokininB receptors potentiates the acoustic startle response in the
771 rat. J Neurosci 17:1838-1847.
772
773 Franklin K, Paxinos G (2007) The Mouse Brain in Stereotaxic Coordinates. San Diego,
774 California: Academic Press.
775
776 Gentet LJ, Stuart GJ, Clements JD (2000) Direct measurement of specific membrane
777 capacitance in neurons. Biophys J 79:314-320.

778 Giovanoli S, Engler H, Engler A, Richetto J, Voget M, Willi R, Winter C, Riva MA,
779 Mortensen PB, Feldon J, Schedlowski M, Meyer U (2013) Stress in puberty unmasks
780 latent neuropathological consequences of prenatal immune activation in mice. Science
781 339:1095-1099.

782 Golden SA, Covington HE 3rd, Berton O, Russo SJ (2011) A standardized protocol for
783 repeated social defeat stress in mice. Nat Protoc 6:1183-1191
784
785 Goussakov I, Chartoff EH, Tsvetkov E, Gerety LP, Meloni EG, Carlezon WA Jr,
786 Bolshakov VY (2006) LTP in the lateral amygdala during cocaine withdrawal. Eur J
787 Neurosci 23:239-250.
788
789 Hadjkacem I, Ayadi H, Turki M, Yaich S, Khemekhem K, Walha A, Cherif L, Moalla Y,
790 Ghribi F (2016) Prenatal, perinatal and postnatal factors associated with autism
791 spectrum disorder. J Pediatr 92:595-601.
792
793 Harvey L, Boksa P. (2012) Prenatal and postnatal animal models of immune activation:
794 relevance to a range of neurodevelopmental disorders. Dev Neurobiol 72: 1335-1348.

795 Hussman JP (2001) Suppressed GABAergic inhibition as a common factor in suspected
796 etiologies of autism. J Autism Dev Disord 31:247-248.
797
798 Hübner C, Bosch D, Gall A, Lüthi A, Ehrlich I (2014) Ex vivo dissection of
799 optogenetically activated mPFC and hippocampal inputs to neurons in the basolateral
800 amygdala: implications for fear and emotional memory. Front Behav Neurosci 8:64.

JNeurosci Accepted Manuscript

Kawai T, Akira S (2008) Toll-like receptor and RIG-I-like receptor signaling. Ann NY Acad Sci 1143:1-20.

Knuesel I, Chicha L, Britschgi M, Schobel SA, Bodmer M, Hellings JA Toovey S, Prinssen EP (2014) Maternal immune activation and abnormal brain development across CNS disorders. Nat Rev Neurol 10:643-660.

Krstic D, Madhusudan A, Doehner J, Vogel P, Notter T, Imhof C, Manalastas A, Hilfiker M, Pfister S, Schwerdel C, Riether C, Meyer U, Knuesel I (2012) Systemic immune challenges trigger and drive Alzheimer-like neuropathology in mice. J Neuroinflammation 9:151.

LeDoux JE (2000) Emotion circuits in the brain. Annu Rev Neurosci 23:155-184.

Lee E, Lee J, Kim E (2017) Excitation/inhibition imbalance in animal models of autism spectrum disorders. Biol Psychiatry 81:838-847.

Lezak KR, Missig G, Carlezon WA Jr. (2017) Behavioral methods to study anxiety in rodents. Dialogues Clin Neurosci 19:79-89.

Li Y, Meloni EG, Carlezon WA Jr, Milad MR, Pitman RK, Nader K, Bolshakov VY (2013) Learning and reconsolidation implicate different synaptic mechanisms. Proc Natl Acad Sci USA 110:4798-4803.

Lombardo MV, Moon HM, Su J, Palmer TD, Courchesne E, Pramparo T (2017) Maternal immune activation dysregulation of the fetal brain transcriptome and relevance to the pathophysiology of autism spectrum disorder. Mol Psychiatry (Epub ahead of print).

Luchkina NV, Bolshakov VY (2017) Diminishing fear: Optogenetic approach toward understanding neural circuits of fear control. Pharmacol Biochem Behav (Epub ahead of print).

Maren S, Quirk GJ (2004) Neuronal signalling of fear memory. Nat Rev Neurosci 5: 844-852.

Markram K, Markram H (2010) The intense world theory - a unifying theory of the neurobiology of autism. Front Hum Neurosci 4:224.

McDougle CJ, Landino SM, Vahabzadeh A, O'Rourke J, Zurcher NR, Finger BC, Palumbo ML, Helt J, Mullett JE, Hooker JM, Carlezon WA Jr (2015) Toward an immune-mediated subtype of autism spectrum disorder. Brain Res 1617:72-92.

Meltzer A, Van de Water J (2017) The role of the immune system in autism spectrum disorder. Neuropsychopharmacology 42:284-298.

JNeurosci Accepted Manuscript

Miller AH, Haroon E, Felger JC (2017) The immunology of behavior-exploring the role of the immune system in brain health and illness. Neuropsychopharmacology 42:1-4.

Monk CS, Weng SJ, Wiggins JL, Kurapati N, Louro HM, Carrasco M, Maslowsky J, Risi S, Lord C (2010) Neural circuitry of emotional face processing in autism spectrum disorders. J Psychiatry Neurosci 35:105-114.

Mrozek-Budzyn D, Majewska R, Kieltyka A (2013) Prenatal, perinatal and neonatal risk factors for autism – study in Poland. Cent Eur J Med 8:424-430.

Nelson SB, Valakh V (2015) Excitatory/Inhibitory balance and circuit homeostasis in autism spectrum disorders. Neuron 87:684-698.

Onore C, Careaga M, Ashwood P (2012) The role of immune dysfunction in the pathophysiology of autism. Brain Behav Immun 26:383-392.

O'Roak BJ et al. (2012) Multiplex targeted sequencing identifies recurrently mutated genes in autism spectrum disorders. Science 338:1619-1622.

Pape HC, Pare D (2010) Plastic synaptic networks of the amygdala for the acquisition, expression, and extinction of conditioned fear. Physiol Rev 90:419-463.

Patel S, Masi A, Dale RC, Whitehouse AJO, Pokorski I, Alvares GA, Hickie IB, Breen E, Guastella AJ (2017) Social impairments in autism spectrum disorder are related to maternal immune history profile. Mol Psychiatry (Epub ahead of print).

Patterson PH (2009) Immune involvement in schizophrenia and autism: etiology, pathology and animal models. Behav Brain Res 204:313-321.

Petreanu L, Mao T, Sternson SM, Svoboda K (2009) The subcellular organization of neocortical excitatory connections. Nature 457:1142-1145.

Perez de la Mora M, Lara-Garcia D, Jacobsen KX, Vazquez-Garcia M, Crespo-Ramirez M, Flores-Gracia C, Escamilla-Marvan E, Fuxe K (2006) Anxiolytic-like effects of the selective metabotropic glutamate receptor 5 antagonist MPEP after its intra-amygdaloid microinjection in three different non-conditioned rat models of anxiety. Eur J Neurosci 23:2749-2759.

Reisinger S, Khan D, Kong E, Berger A, Pollak A, Pollak DD (2015) The poly(I:C)-induced maternal immune activation model in preclinical neuropsychiatric drug discovery. Pharmacol Ther 149:213-226.

Riccio A, Li Y, Moon J, Kim KS, Smith KS, Rudolph U, Gapon S, Yao GL, Tsvetkov E, Rodig SJ, Van't Veer A, Meloni EG, Carlezon WA Jr, Bolshakov VY, Clapham DE (2009)

JNeurosci Accepted Manuscript

Essential role for TRPC5 in amygdala function and fear-related behavior. Cell 137:761-772.

Riccio A, Li Y, Tsvetkov E, Gapon S, Yao GL, Smith KS, Engin E, Rudolph U, Bolshakov VY, Clapham DE (2014) Decreased anxiety-like behavior and Gαq/11-dependent responses in the amygdala of mice lacking TRPC4 channels. J Neurosci 34:3653-3667.

Rinaldi T, Perrodin C, Markram H (2008) Hyper-connectivity and hyper-plasticity in the medial prefrontal cortex in the valproic Acid animal model of autism. Front Neural Circuits 2:4.

Rubenstein JL, Merzenich MM (2003) Model of autism: increased ratio of excitation/inhibition in key neural systems. Genes Brain Behav 2:255-267.

Rudie JD, Shehzad Z, Hernandez LM, Colich NL, Bookheimer SY, Iacoboni M, Dapretto M (2012) Reduced functional integration and segregation of distributed neural systems underlying social and emotional information processing in autism spectrum disorders. Cereb Cortex 22:1025-1037.

Sah P, Faber ESL, Lopez De Armentia M, Power J (2003) The amygdaloid complex: anatomy and physiology. Physiol Rev 83:803-834.

Sanders SK, Shekhar A (1995) Regulation of anxiety by GABAA receptors in the rat amygdala. Pharmacol Biochem Behav 52:701-706.

Sangha S, Greba Q, Robinson PD, Ballendine SA, Howland JG (2014) Heightened fear in response to a safety cue and extinguished fear cue in a rat model of maternal immune activation. Front Behav Neurosci 8:168.

Semple BD, Blomgren K, Gimlin K, Ferriero DM, Noble-Haeusslein LJ (2013) Brain development in rodents and humans: Identifying benchmarks of maturation and vulnerability to injury across species. Prog Neurobiol 106-107:1-16.

Sholl DA (1953) Dendritic organization in the neurons of the visual and motor cortices of the cat. J Anat 87:387-406.

Smith SE, Li J, Garbett K, Mirnics K, Patterson PH (2007) Maternal immune activation alters fetal brain development through interleukin-6. J Neurosci 27:10695-10702.

South M, Rodgers J (2017) Sensory, emotional and cognitive contributions to anxiety in autism spectrum disorders. Front Hum Neurosci 11:20.

Strobel C, Marek R, Gooch HM, Sullivan RK, Sah P (2015) Prefrontal and auditory input to intercalated neurons of the amygdala. Cell Rep 10:1435-1442.

JNeurosci Accepted Manuscript

936 Sui L, Chen M (2012) Prenatal exposure to valproic acid enhances synaptic plasticity in
937 the medial prefrontal cortex and fear memories. Brain Res Bull 87:556-563.
938
939 Talkowski ME, Minikel EV, Gusella JF (2014) Autism spectrum disorder genetics:
940 diverse genes with diverse clinical outcomes. Harv Rev Psychiatry 22:65-75.

941 Testa-Silva G, Loebel A, Giugliano M, de Kock CP, Mansvelder HD, Meredith RM
942 (2012) Hyperconnectivity and slow synapses during early development of medial
943 prefrontal cortex in a mouse model for mental retardation and autism. Cereb Cortex 22:
944 1333-1342.

945 Tsvetkov E, Carlezon WA, Benes FM, Kandel ER, Bolshakov VY (2002) Fear
946 conditioning occludes LTP-induced presynaptic enhancement of synaptic transmission
947 in the cortical pathway to the lateral amygdala. Neuron 34:289-300.
948
949 Vila-Verde C, Marinho AL, Lisboa SF, Guimarães FS (2016) Nitric oxide in the prelimbic
950 medial prefrontal cortex is involved in the anxiogenic-like effect induced by acute
951 restraint stress in rats. Neuroscience 320:30-42.
952
953 Werling DM, Geschwind DH (2013) Sex differences in autism spectrum disorders. Curr
954 Opin Neurol 26:146-153.
955
956 Zerbo O, Iosif AM, Delwiche L, Walker C, Hertz-Picciotto I.Knuesel (2011) Month of
957 conception and risk of autism. Epidemiology 22:469-475.
958
959 Zucker RS, Regehr WG (2002) Short-term synaptic plasticity. Annu Rev Physiol 64:
960 355-405.
961

962

963 **Figure Legends**

964 **Figure 1.** Immune activation is associated with activation of microglia in the BLA and
965 ASD-related behavioral dysfunctions. ***A***, Experimental design (see the main text for
966 details). ***B***, Confocal microscopic images showing immunohistochemical staining for
967 Ionized calcium binding adaptor molecule 1 (IBA-1), a microglial marker, in the
968 basolateral nucleus of the amygdala (BLA) in 13-week old offspring mice from different
969 experimental groups. ***C***, The number of IBA-1 positive cells and immunoreactivity (IR)
970 of IBA-1 were increased in the offspring groups receiving the postnatal LPS injections,

JNeurosci Accepted Manuscript

971 indicating a robust activation of microglia ~12 weeks after the LPS injection at PND9
972 (Veh_Veh group: *n* = 6 slides from 4 mice; Poly I:C_Veh: *n* = 8 slides from 4 mice;
973 Veh_LPS: *n* = 5 slides from 3 mice; Poly I:C_LPS: *n* = 3 slides from 3 mice). ***D***,
974 Quantitative morphological analysis of microglia in the animal models of maternal and
975 postnatal immunoactivation. Left, there was no difference in the soma size of microglia
976 in the BLA between experimental groups (Veh-Veh group: *n* = 50 from 4 mice; Poly
977 I:C_Veh: *n* = 59 from 4 mice; Veh_LPS: *n* = 93 from 7 mice; Poly I:C_LPS: *n* = 36 from
978 3 mice). Right, the groups did not differ in the number of microglial ramifications (Veh-
979 Veh group: *n* = 50 from 4 mice; Poly I:C_Veh: *n* = 59 from 4 mice; Veh_LPS: *n* = 93
980 from 7 mice; Poly I:C_LPS: *n* = 36 from 3 mice). ***E***, Results of the open field test. Left,
981 summary plot showing the percentage of time spent in the center of the arena.
982 Increased anxiety-like behavior (less time spent in the center) was observed in
983 Veh_LPS and Poly I:C_LPS groups relative to the control Veh_Veh group. Right, plot
984 showing the total distance traveled during the open field test. The number of mice
985 tested: Veh-Veh group: *n* = 28 mice; Poly I:C_Veh: *n* = 26 mice; Veh_LPS: *n* = 11 mice;
986 Poly I:C_LPS: *n* = 17 mice. ***F***, Results of the social interaction test. Left, mice in
987 Veh_LPS and Poly I:C_LPS groups showed impaired social behavior as they spent less
988 time in the interaction zone with the novel conspecific mouse relative the control
989 Veh_Veh group. Right, distance traveled during the social interaction test. The number
990 of mice tested: Veh-Veh group: *n* = 12 mice; Poly I:C_Veh: *n* = 17 mice; Veh_LPS: *n* =
991 11 mice; Poly I:C_LPS: *n* = 18 mice. Error bars are SEM.
992

JNeurosci Accepted Manuscript

Figure 2. Optogenetic analysis of mPFC inputs to the BLA in animal models of maternal and postnatal immunoactivation. ***A***, Experimental design for optogenetic activation of mPFC-amygdala projections. A vertical dashed line indicates location of a coronal section shown in *E* (as in Cho et al., 2013). ***B***, Left, a microscopic image at the low magnification shows the expression of eYFP-ChR2 at the injection site in mPFC (green) merged with an image of fluorescent Nissl stain (red); Right: a confocal image showing expression of eYFP-ChR2 across the cell layers in the PL. PL, prelimbic cortex; IL, infralimbic cortex; aca, anterior commissure, anterior part. ***C***, Left, ChR2-mediated currents recorded in a pyramidal neuron in layer V of mPFC were evoked by 1-s pulses of blue light (470 nm, blue horizontal bar) of increasing intensity (0.2 – 1.7 mW/mm^2) in the presence of NBQX (10 μM), D-AP5 (50 μM) and bicuculline (30 μM). Right, input-output plots of the photocurrent amplitudes as a function of the light power densities (mW/mm^2) in slices from different experimental groups (Veh_Veh group: *n* = 21 neurons from 8 mice; Poly I:C_Veh: *n* = 22 neurons from 9 mice; Veh_LPS: *n* = 17 neurons from 7 mice; Poly I:C_LPS: *n* = 23 neurons from 10 mice). Expression of ChR2 in the mPFC was not affected by immunoactivation. ***D***, Left, examples of action potentials recorded in a pyramidal neuron in layer V of mPFC triggered by trains of 1-ms pulses of blue light at different stimulation frequencies (5 - 40 Hz, marked by vertical blue bars for the 5 Hz stimulation) in current-clamp mode. Right, plot of AP firing reliability at different stimulation frequencies (Veh_Veh group: *n* = 9 neurons from 4 mice; Poly I:C_Veh: *n* = 8 neurons from 5 mice; Veh_LPS: *n* = 6 neurons from 4 mice; Poly I:C_LPS: *n* = 7 neurons from 5 mice).

JNeurosci Accepted Manuscript

Figure 3. mPFC-amygdala synaptic connectivity and innervation patterns of the amygdala by ChR2-expressing mPFC projection fibers. ***A***, Light-evoked EPSCs recorded in BLA principal neurons at –80 mV were blocked by the AMPA/kainate receptor antagonist NBQX (10 μM). ***B***, Fractions of neurons in BLA and dITC in which EPSCs could be observed in response to photostimulation of mPFC afferents in slices from all groups. In these recordings, the light power density was 10.5 mW/mm^2 (BLA: *n* = 38 neurons from 38 recorded cells in Veh_Veh group, *n* = 30 neurons from 30 recorded cells in Poly I:C_Veh group, *n* = 36 neurons from 36 recorded cells in Veh_LPS group, *n* = 36 neurons from 36 recorded cells in Poly I:C_LPS group; dITC: *n* = 8 neurons from 9 recorded cells in Veh_Veh group, *n* = 5 neurons from 7 recorded cells in Poly I:C_Veh group, *n* = 6 neurons from 7 recorded cells in Veh_LPS group, *n* = 8 neurons from 10 recorded cells in Poly I:C_LPS group. ***C***, Rescue of optogenetically-induced and tetrodotoxin (TTX)-blocked EPSCs at mPFC(PL)-BLA projections by aminopyridine (4-AP). Left, a graph showing the time course of changes in the EPSC amplitude under control conditions (1), after application of TTX (2) and after the subsequent addition of 4-AP (3). Right, EPSCs (average of 10 traces) recorded in a BLA neuron at –80 mV under different experimental conditions. EPSCs evoked by photostimulation (with 5- ms-long pulses) of ChR2-expressing mPFC fibers were blocked by TTX (1 μM). An addition of 4-AP (1 mM) in the presence of TTX partially rescued the EPSC (as in ref. 29; n = 3 neurons), confirming monosynaptic nature of activated mPFC-BLA projections. ***D***, Summary plot of the EPSC amplitudes in TTX only and TTX + 4-AP. Peak amplitudes of EPSCs were normalized to the baseline

JNeurosci Accepted Manuscript

EPSC recorded under control conditions. Open circles represent individual experiments whereas closed circles show average values (n = 3 neurons). ***E***, Experimental design for the analysis of mPFC- amygdala connectivity. Vertical lines indicate location of coronal sections through the amygdala shown in ***F***. ***F***, Microscopic images showing innervation of the amygdala by ChR2-eYFP expressing mPFC fibers (green) in coronal brain sections (300 μm in thickness) along the rostral-caudal axis. Blue fluorescence indicates DAPI counter-stain. LA, lateral nucleus of the amygdala; BLA, the basolateral nucleus of the amygdala; CeL, lateral division of the central nucleus of the amygdala; CeM, medial division of the central nucleus; dITC, dorsal cluster of intercalated cells in the amygdala. ***G***–***I***, Mean densities of ChR2-eYFP fluorescence due to the innervation by mPFC projections in different sections along the rostral-caudal axes in BLA (***G***), LA (***H***) and CeA (***I***) in slices from all experimental groups (Veh_Veh group: *n* = 16 slides from 6 mice; Poly I:C_Veh: *n* = 14 slides from 4 mice; Veh_LPS: *n* = 18 slides from 6 mice; Poly I:C_LPS: *n* = 17 slides from 6 mice).

Figure 4. Maternal immunoactivation (MIA) but not postnatal immunoactivation (PIA) results in increased synaptic strength in glutamatergic mPFC projections to the BLA. ***A***, Experimental design for optogenetic analysis of mPFC- amygdala projections. A vertical line indicates location of a coronal section through the amygdala shown in ***B***. ***B***, Left, a confocal microscopic image showing ChR2-eYFP-expressing mPFC fibers in the amygdala (green). Red fluorescent cells in the BLA are neurobiotin-filled neurons. Right, a higher magnification image of the same section. ***C***, EPSCs (average of five responses) recorded in principal neurons (PN) in mPFC-BLA projections in voltage-

JNeurosci Accepted Manuscript

clamp mode at a holding potential –80 mV in slices from different experimental groups. EPSCs were evoked by photostimuli of increasing intensity. ***D***, Input-output plots for peak amplitudes of EPSCs at the mPFC-BLA synapses in all experimental groups (Veh-Veh group: *n* = 39 neurons from 12 mice; Poly I:C_Veh: *n* = 28 neurons from 9 mice; Veh_LPS: *n* = 36 neurons from 9 mice; Poly I:C_LPS: *n* = 38 neurons from 12 mice). ***E***, EPSC in BLA principal neurons were evoked by paired photostimuli (50-ms inter-pulse interval) at the saturating photostimulation intensity (10.2 mW/mm^2) in slices from all groups. ***F***, There was no effect of the treatments on the PPR magnitude (Veh-Veh group: *n* = 25 neurons from 12 mice; Poly I:C_Veh: *n* = 24 neurons from 9 mice; Veh_LPS: *n* = 16 neurons from 9 mice; Poly I:C_LPS: *n* = 28 neurons from 12 mice). ***G***, Examples of sEPSCs recorded in BLA neurons. ***H*** and ***I***, Cumulative amplitude (***H***) and inter-event interval (***I***) histograms of sEPSCs recorded in slices from all groups. ***J*** and ***K***, Summary plots of the mean sEPSC amplitude (***J***) and the frequency (***K***) in slices from all groups (Veh_Veh group: *n* = 10 neurons from 5 mice; Poly I:C_Veh: *n* = 9 neurons from 6 mice; Veh_LPS: *n* = 8 neurons from 4 mice; Poly I:C_LPS: *n* = 9 neurons from 5 mice).

Figure 5. Sholl analysis of dendritic morphology in the BLA following immune activation. ***A***, Sholl dendritic analysis of reconstructed neurobiotin-filled BLA neurons was performed by placing a series of concentric circles, spaced at 30-μm intervals, centered on the soma. ***B***, The average soma size estimates in all experimental groups. There was a significant increase in the soma size in LPS-treated mice (see text for details). ***C***, Averaged number of primary dendrites in all experimental groups. ***D***,

JNeurosci Accepted Manuscript

Summary plot of the dendritic length as a function of the radial distance from soma by 30-μm increments. There was a main effect of LPS on the dendritic length: three-way ANOVA (Poly I:C x LPS x distance from soma), Poly I:C, $F_{(1,224)} = 0.272$, $p = 0.603$; LPS, $F_{(1,224)} = 10.499$, $p = 0.001$; interaction, $F_{(7,224)} = 0.64$, $p = 1.0$; post-hoc *Bonferonni's* test: $p = 0.004$ for Veh_Veh versus Veh_LPS. ***E***, Summary plot of the dendritic surface area as a function of the radial distance from soma. There was an increase in the dendritic surface area in Veh_LPS and Poly I:C_LPS groups versus Veh_Veh group: three-way ANOVA (Poly I:C x LPS x distance from soma), Poly I:C, $F_{(1,224)} = 1.681$, $p = 0.196$; LPS, $F_{(1,224)} = 51.762$, $p < 0.001$; interaction, $F_{(1,224)} = 0.086$, $p = 0.99$; post-hoc *Bonferonni's* test: $p < 0.001$ for both Veh_Veh versus Veh_LPS and Veh_Veh versus Poly I:C_LPS groups. ***F***, The averaged number of branch points. There was no difference in branch point numbers between the groups: three-way ANOVA (Poly I:C x LPS x distance from soma), Poly I:C, $F_{(1,224)} = 2.27$, $p = 0.133$; LPS, $F_{(1,224)} = 0.0396$, $p = 0.842$; interaction, $F_{(7,224)} = 0.338$, $p = 0.936$. ***G***, Averaged dendritic diameter as a function of distance from soma. There was an increase in the averaged dendritic diameter in the Veh_LPS and Poly I:C_LPS groups versus Veh_Veh group: three-way ANOVA (Poly I:C x LPS x distance from soma), Poly I:C, $F_{(1,112)} = 7.5$, $p = 0.007$; LPS, $F_{(1,112)} = 30.197$, $p < 0.001$; interaction, $F_{(3,112)} = 0.376$, $p = 0.771$; post-hoc *Bonferonni's* simultaneous multiple comparisons: $p = 0.032$ for Veh_Veh versus Veh_LPS and $p < 0.001$ for Veh_Veh group versus Poly I:C_LPS group). Veh-Veh group: n = 8 neurons from 5 mice; Poly I:C_Veh : n = 8 neurons from 4 mice; Veh_LPS: n = 8 neurons from 7 mice; Poly I:C_LPS: n = 8 neurons from 6 mice.

JNeurosci Accepted Manuscript

Figure 6. Feed-forward inhibition in the mPFC-BLA pathway is diminished in postnatally immunoactivated mice. ***A***, Experimental design for analyzing neural circuits of feed-forward inhibition in the mPFC-BLA projections. Glutamatergic inputs to both BLA principal neurons (PN) and interneurons (IN), activated by blue light stimulation of mPFC fibers, were blocked by AMPA and NMDA receptor antagonists (10 μM NBQX and 50 μM D-AP5, respectively). Projections from IN to PN were suppressed by the $GABA_A$ receptor antagonist bicuculline (Bic, 30 μM). ***B***, Left, synaptic responses were induced by photostimualtion (7.4 – 10.2 mW/mm^2) and recorded in BLA neurons at -80 mV (black trace, EPSC) and 0 mV (red trace, IPSC). The inset shows a delayed onset (synaptic latency) of synaptic currents recorded at 0 mV. Right, mean synaptic latencies of IPSCs and EPSCs. The IPSC latency (at a holding potential of 0 mV) was much longer compared to EPSCs recorded in the same neurons at a holding potential of –80 mV, suggesting that the IPSC is polysynaptic in nature (*n* = 10 neurons from 3 mice). ***C***, IPSCs at a holding potential of 0 mV were completely blocked by the $GABA_A$ receptor antagonist bicuculline (30 μM). ***D***, Both EPSCs and IPSCs (recorded in BLA principal neurons at -80 mV or 0 mV, respectively) were completely blocked by NBQX (10 μM) and D-AP5 (50 μM), confirming that the IPSCs, mediated by activation of local circuit interneurons, are polysynaptic in origin and triggered by glutamatergic mPFC inputs to IN. ***E***, EPSCs and IPSCs (averages of 10 traces) recorded in the same neurons in slices from all experimental groups. IPSCs were normalized to the mean amplitude of the EPSC at a holding potential of –80 mV to allow the comparison of changes in the IPSC amplitude between the groups. ***F***, The IPSC/EPSC amplitude ratio was decreased in Veh_LPS and Poly I:C_LPS groups, indicating an effect of PIA on the

JNeurosci Accepted Manuscript

1130 balance between excitation and inhibition in mPFC-BLA projections (Veh_Veh group: *n*
1131 = 17 neurons from 7 mice; Poly I:C_Veh: *n* = 18 neurons from 9 mice; Veh_LPS: *n* = 13
1132 neurons from 5 mice; Poly I:C_LPS: *n* = 23 neurons from 11 mice). ***G***,
1133 Immunoactivation had no effect on the latencies of EPSCs or IPSCs in mPFC-BLA
1134 projections (Veh_Veh group: *n* = 17 neurons from 7 mice; Poly I:C_Veh: *n* = 18 neurons
1135 from 9 mice; Veh_LPS: *n* = 13 neurons from 5 mice; Poly I:C_LPS: *n* = 23 neurons from
1136 11 mice).
1137
1138 **Figure 7.** Neuroinflammation is associated with the increased probability of
1139 synaptically-driven spike firing in the mPFC-BLA pathway. ***A***, Experimental design for
1140 recording of synaptically-driven extracellular spikes in BLA principal neurons in
1141 response to photostimulation of mPFC fibers. ***B***, Left, superimposed synaptic
1142 responses (extracellular spikes) recorded in a BLA principal neuron evoked by
1143 photostimulation of ChR2-expressing mPFC fibers in a cell-attached patch
1144 configuration. Right, recordings under current clamp conditions from the same neuron
1145 after establishing a whole-cell recording configuration. ***C***, Examples of responses
1146 (extracellular spikes recorded in a cell-attached patch configuration) in BLA neurons to
1147 light pulses of increasing intensity under control conditions (left) and in the presence of
1148 the $GABA_A$ receptor antagonist bicuculline (30 μM, right). ***D***, The number of spikes in
1149 response to presynaptic photostimulation was increased significantly in the presence of
1150 the $GABA_A$ receptor antagonist bicuculline (30 μM) in the external medium (control: *n* =
1151 10 neurons from 3 mice; bicuculline: *n* = 6 neurons from 3 mice). ***E***, Examples of
1152 synaptically-driven spikes in BLA principal neurons in slices from different groups of

JNeurosci Accepted Manuscript

mice. ***F***, Summary input-output plots for synaptically-driven spikes in BLA neurons in all experimental groups (Veh_Veh group: *n* = 22 neurons from 7 mice; Poly I:C_Veh: *n* = 13 neurons from 5 mice; Veh_LPS: *n* = 21 neurons from 5 mice; Poly I:C_LPS: *n* = 22 neurons from 7 mice).

Figure 8. Functional alterations in the mPFC-BLA circuits associated with maternal and postnatal immunoactivation. ***A***–***D***, Left in each panel, diagrams illustrate the signal flow in the mPFC-BLA pathways in mice from all experimental groups. Glutamatergic (red lines) mPFC projections form excitatory synapses on BLA principal neurons (PNs) as well as on the local circuit interneurons (INs). Interneurons form inhibitory synapses (blue line) on PN, and thus provide strong feed-forward inhibition in the mPFC-BLA pathway. PNs in the BLA, when driven to the AP threshold, send information (red line) to the downstream structures, including the central nucleus of the amygdala (CeA), bed nucleus of the stria terminalis (BNST), striatum, and cortical areas. Right, activation of mPFC inputs to BLA PNs and INs results in generation of monosynaptic EPSCs (black trace) and disynaptic IPSCs (blue trace), which could be recorded in BLA PNs at holding potentials of –80 mV or 0 mV, respectively. Changes in the thickness of lines indicate a change in synaptic efficacy. See Discussion for the additional detailed interpretation of experimental findings.

Table 1. Summary table of passive membrane properties determined in current-clamp recordings from principal neurons in slices of the BLA from different experimental groups of mice. The membrane capacitance (Cm) was calculated using the equation,

JNeurosci Accepted Manuscript

1176 $C_m = \tau(1/R_a + 1/R_{in})$ as previously described (Gentet et al., 2000). Two-way ANOVA in
1177 a 2x2 factorial design was used to evaluate the statistical significance of differences
1178 between experimental groups.
1179
1180

JNeurosci Accepted Manuscript

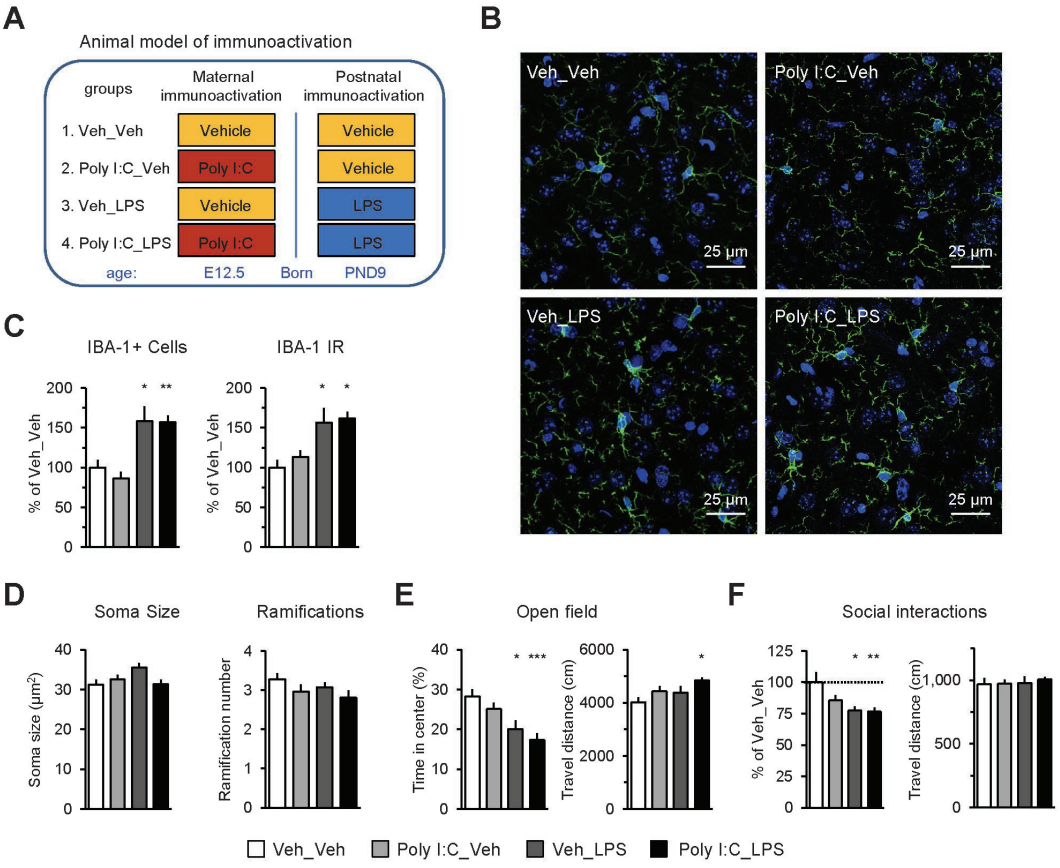

Fig. 1
Li et al.

JNeurosci Accepted Manuscript

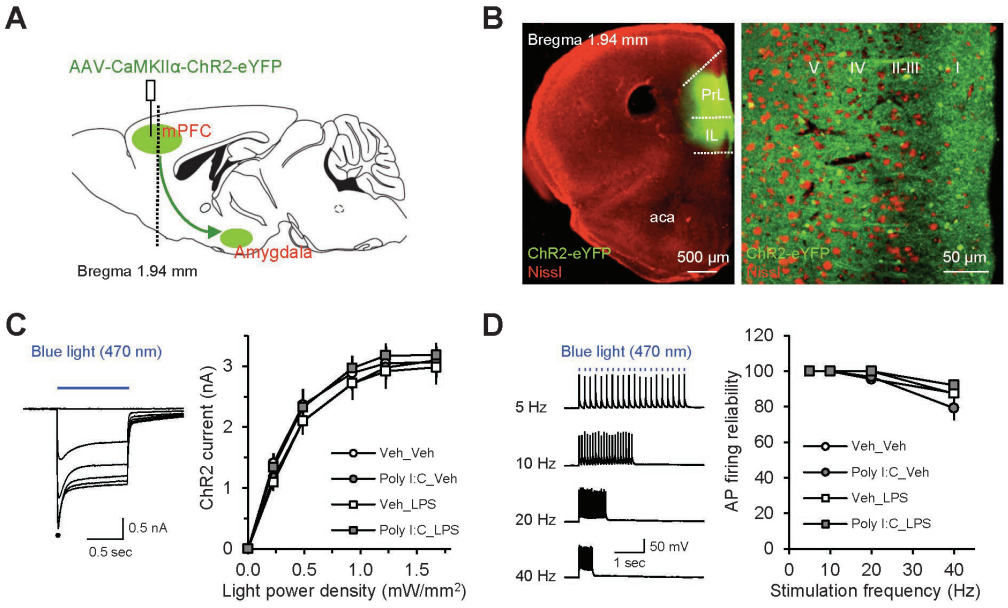

Fig. 2
Li et al.

JNeurosci Accepted Manuscript

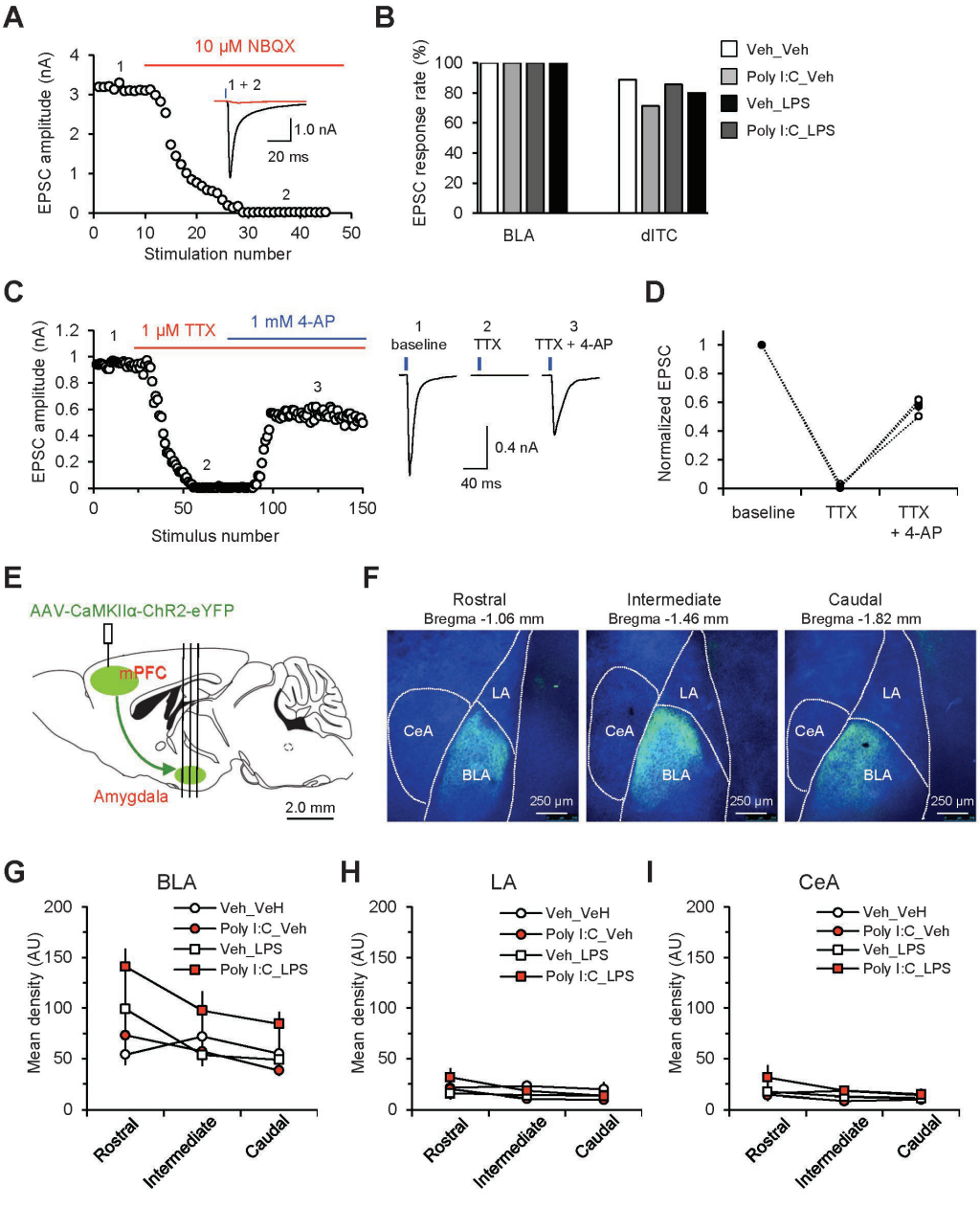

Figure 3
Li et al.

JNeurosci Accepted Manuscript

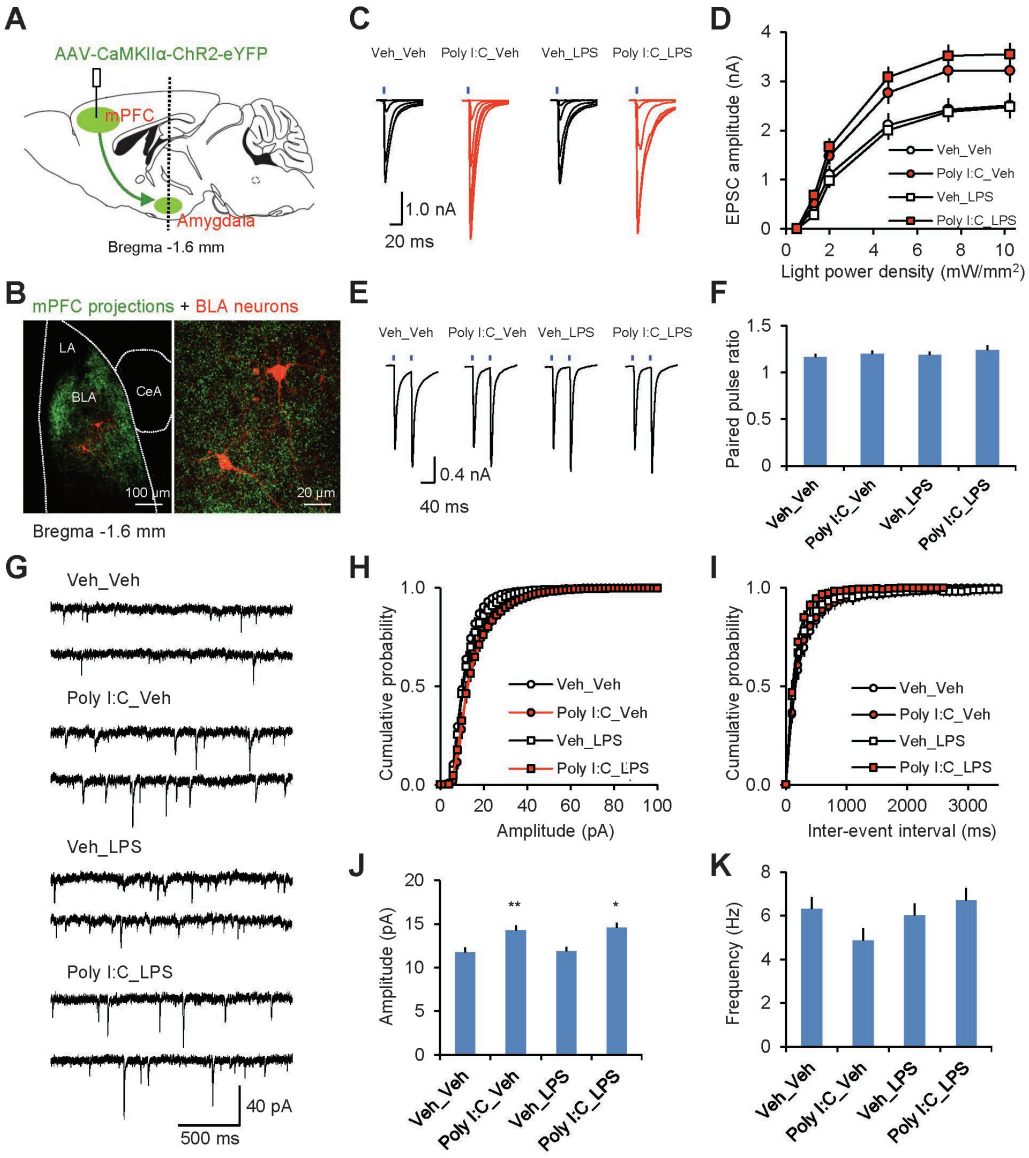

Fig. 4
Li et al.

JNeurosci Accepted Manuscript

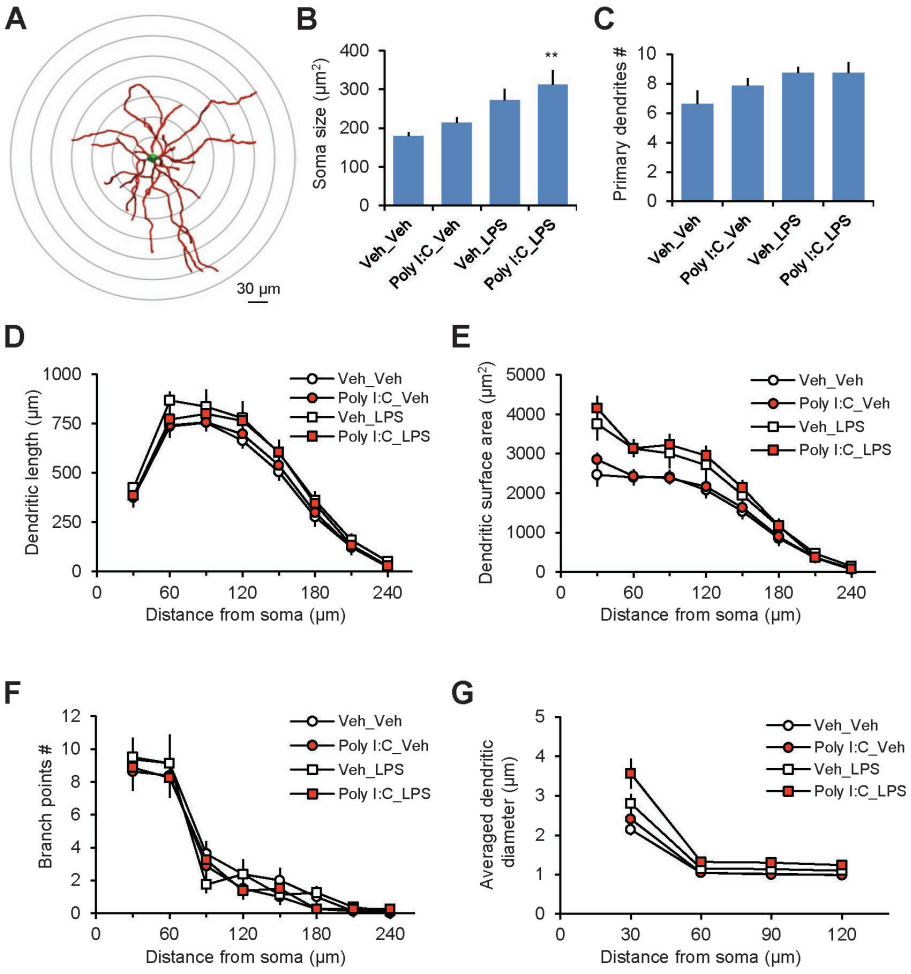

Fig. 5
Li et al.

JNeurosci Accepted Manuscript

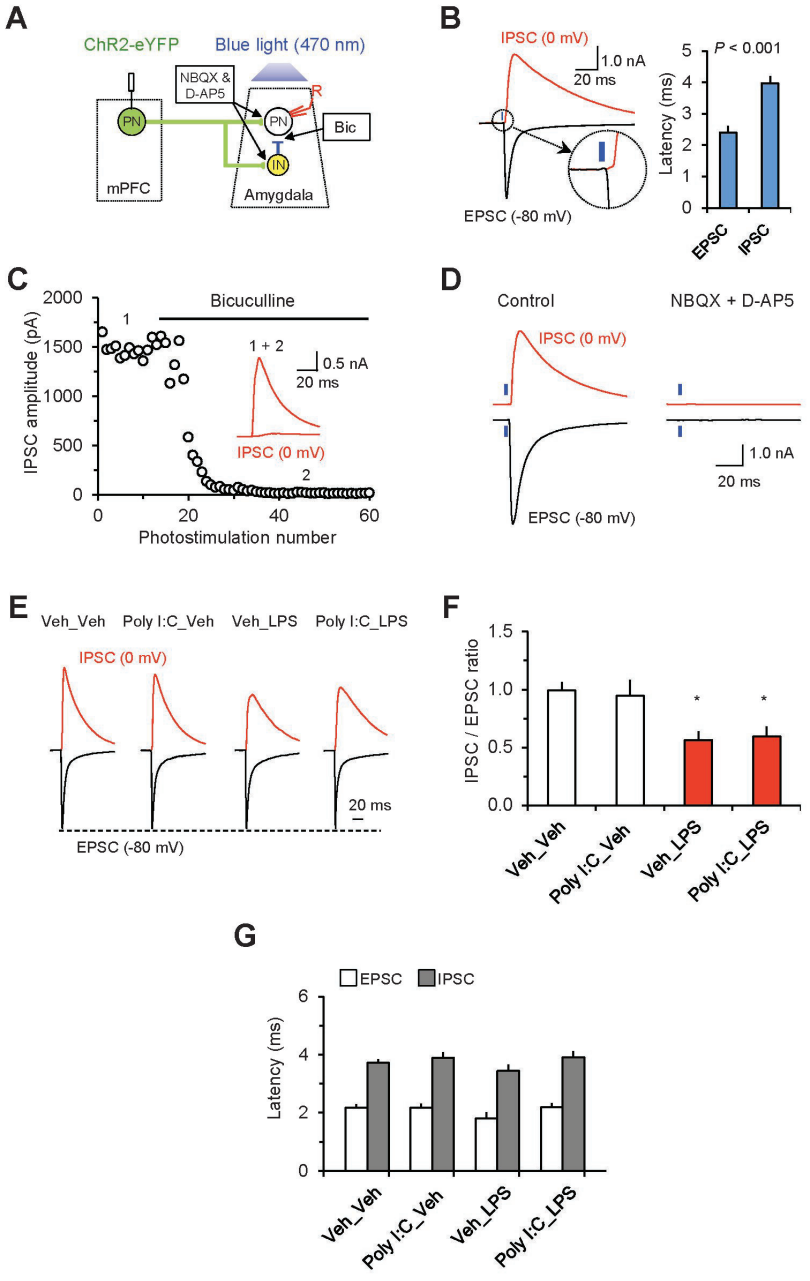

Fig. 6
Li et al.

JNeurosci Accepted Manuscript

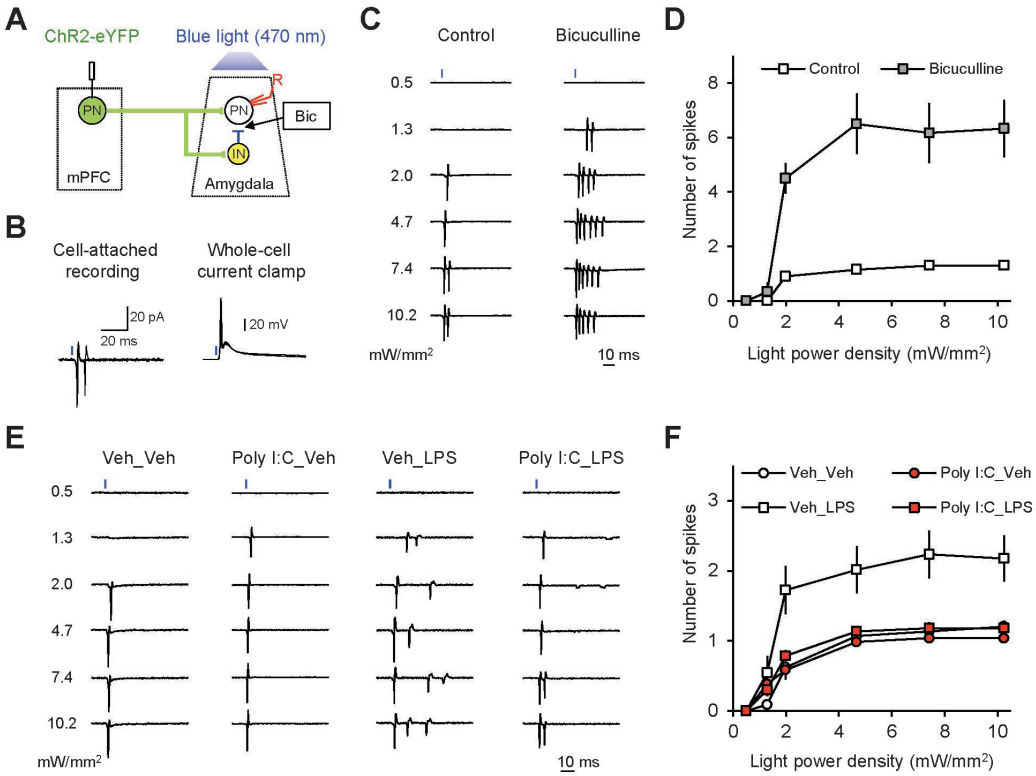

Fig. 7
Li et al.

JNeurosci Accepted Manuscript

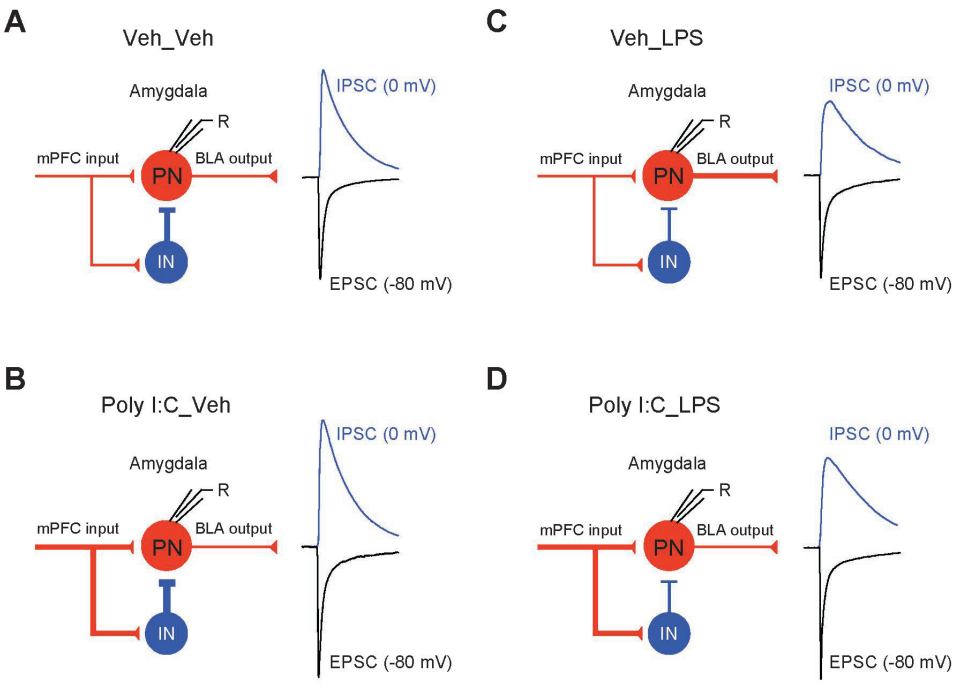

Fig. 8
Li et al.

JNeurosci Accepted Manuscript

Table 1. Summary table of passive membrane properties determined in current-clamp recordings from principal neurons in slices of the BLA from different experimental groups of mice

Group	Veh_Veh	Poly I:C_Veh	Veh_LPS	Poly I:C_LPS	Poly I:C	LPS
Cell #/Mice #	21/10	24/11	15/7	20/12		
R_{series} (MΩ)	17.2 ± 0.7	16.5 ± 0.6	17.1 ± 1.0	17.5 ± 0.8	$F_{(1, 76)} = 0.03$ $p = 0.871$	$F_{(1, 76)} = 0.29$ $p = 0.59$
R_{input} (MΩ)	159.3 ± 12.5	155.4 ± 16.4	152.0 ± 14.5	131.0 ± 12.8	$F_{(1, 76)} = 0.71$ $p = 0.402$	$F_{(1, 76)} = 1.16$ $p = 0.285$
RMP (mV)	74.2 ± 0.9	76.1 ± 1.1	76.6 ± 1.6	72.5 ± 1.1	$F_{(1, 76)} = 0.87$ $p = 0.355$	$F_{(1, 76)} = 0.26$ $p = 0.61$
$\tau_{membrane}$ (ms)	2.7 ± 0.1	3.1 ± 0.1	3.0 ± 0.1	2.9 ± 0.1	$F_{(1, 76)} = 1.05$ $p = 0.308$	$F_{(1, 76)} = 0.41$ $p = 0.526$
C_m (pF)	181.8 ± 9.1	215.3 ± 12.1	204.1 ± 11.8	196.3 ± 7.4	$F_{(1, 76)} = 1.48$ $p = 0.228$	$F_{(1, 76)} = 0.02$ $p = 0.877$